Chapter 5

Quasi-perpendicular Shock Structure and Processes

S. D. Bale[1], M. A. Balikhin[2], T. S. Horbury[3], V. V. Krasnoselskikh[4], H. Kucharek[5], E. Möbius[5 6], S. N. Walker[2], A. Balogh[3], D. Burgess[7], B. Lembège[8], E. A. Lucek[3], M. Scholer[9], S. J. Schwartz[7 10], and M. F. Thomsen[11]

5.1 Introduction

In the two decades prior to the launch of Cluster, collisionless shocks at which the magnetic field in the unshocked plasma is nearly perpendicular to the shock normal ('quasi-perpendicular shocks') received considerable attention. This is due, in part, to their relatively clean, laminar appearance in the time series data. The tendency of the magnetic field to bind particles together owing to their (perpendicular) gyromotion gives rise to this appearance, which facilitated deeper studies into the collisionless processes responsible for the overall thermalization of the principle plasma populations as well as the acceleration of an energetic non-thermal component. Despite the considerable effort, key questions remained unanswered or re-

[1]Department of Physics and Space Sciences Laboratory, University of California, Berkeley, CA, USA
[2]Automatic Control and Systems Engineering, University of Sheffield, Sheffield, UK
[3]Space and Atmospheric Physics, The Blackett Laboratory, Imperial College London, London, UK
[4]LPCE/CNRS, Orléans, France
[5]Space Science Center, Institute for the Study of Earth, Oceans, and Space, University of New Hampshire, Durham, New Hampshire, USA
[6]Also Department of Physics, University of New Hampshire, Durham, New Hampshire, USA
[7]Astronomy Unit, Queen Mary, University of London, London, UK
[8]CETP/IPSL, Velizy, France
[9]Max-Planck-Institut für extraterrestrische Physik, Garching, Germany
[10]Now at Space and Atmospheric Physics, The Blackett Laboratory, Imperial College London, London, UK
[11]Los Alamos National Laboratory, Los Alamos, NM, USA

Space Science Reviews 118: 161–203, 2005.
DOI: 10.1007/s11214-005-3827-0

mained open to interpretation. Single, and at best dual, spacecraft studies were unable to place quantitative limits on the important spatial scales, nor assess the role of non-stationary aspects in the overall shock transition.

By taking advantage of the sharp, quasi-perpendicular shock transitions, Cluster investigations have been able to address the shock orientation and motion via now-standard four spacecraft techniques. As a consequence, Cluster has been able to probe the internal shock scales (and hence physics). Additionally, the multi-spacecraft strategy has enabled definitive studies of where energetic particles do, and don't, come from. This Chapter summarises many of these achievements.

5.2 Structure and Thermalization

5.2.1 Bow shock orientation and global structure

Knowledge of the basic parameters of a shock, such as Mach number and angle θ_{Bn} between the shock normal and (unshocked) magnetic field, is essential for a quantitative analysis of shock dynamics. However, such parameters are often difficult to determine in practice since they require both accurate measurement of plasma and field values around the shock, as well as estimates of characteristics of the shock itself. Most obvious among the latter are the shock orientation and speed. These parameters are difficult to estimate with a single spacecraft, although various techniques such as coplanarity (e.g., Schwartz, 1998) can be used to estimate the shock orientation. New methods of determining shock orientation and speed are therefore of interest.

The measurement of the same shock transition by the four Cluster spacecraft in close succession allows us to estimate the orientation and velocity of the structure in several ways which have not previously been possible. Each of these methods requires assumptions to be made about the properties of the shock, and each has advantages and disadvantages in different situations. A number of such methods have been applied to Cluster crossings of the quasi-perpendicular bow shock, as we report below.

5.2.1.1 Comparison of methods to determine shock orientation

Horbury et al. (2002) used four spacecraft timings of magnetic field data to estimate the orientation of the quasi-perpendicular bow shock at a number of crossings and compare these results with magnetic coplanarity estimates as well as orientations predicted by parametric models of the large scale bow shock shape.

If we assume the shock to be planar on the scale of the spacecraft separations, and to be travelling at a constant speed as it passes over the four spacecraft, then the times at which it crosses them can be used to estimate the normal of the shock plane and the speed at which it is travelling along that normal (see Dunlop and Woodward, 1998, for more details). These assumptions will not always be satisfied. Non-planarity of the shock can be caused by large scale curvature or by rippling

and waves around the shock. Horbury et al. (2002) considered shock crossings in late 2000 and early 2001, when the Cluster spacecraft were typically around 600 km apart, much smaller than the scale of the bow shock curvature around the magnetopause. They also only considered fairly sharp, clean crossings without extensive wave activity, which restricted them to quasi-perpendicular shocks. They rejected any shock with significantly different magnetic field profiles at different spacecraft, or any nearby changes in upstream conditions. For example, acceleration of the shock (discussed in detail in section 5.2.4.4) can often be identified as a different width of the profile at different spacecraft. Horbury et al. (2002) identified such cases, but did not analyse them.

For a reliable estimate of the shock orientation using timings, the error on the relative times at which the shock crossed the four spacecraft should be small. In practice, the finite shock width, combined with the presence of waves around the shock, can result in uncertainty in the shock time of around a second. The need to minimise this uncertainty for the timing method makes relatively sharp quasi-perpendicular crossings much easier to analyse than more oblique, structured shocks. When the Cluster spacecraft are around 100 km apart, the shock can travel between them in one or two seconds, leading to a large fractional error in the relative timings. If the spacecraft are a few thousand km apart, the shock has often changed speed or profile in the tens of seconds it takes to travel between them. In early 2001, however, the spacecraft were typically around 600 km apart at apogee in the solar wind, corresponding to shock crossings around ten seconds apart between spacecraft, resulting in small fractional errors in relative timings. However, with the assumptions used in this method (constant motion, planarity, accurate timings) it is important to test its accuracy before using it routinely.

Horbury et al. (2002) considered 48 quasi-perpendicular shock crossings in 2001, and estimated the speed and orientation of each, using inter-spacecraft timings (see Figure 5.1). They compared the timing-based orientation estimates with those from two models of the bow shock shape (Peredo et al., 1995; Formisano, 1979). They found that the timing-based estimates of the shock orientation agreed very well with the models, with nearly 80% being less than 10° apart (Figure 5.2, left panel). This result implies that both the timing method and the models are usually good estimators of the shock orientation, to around 10° accuracy. Indeed, the accuracy of the timing-based estimates can be seen qualitatively from the consistency of the normals shown in Figure 5.1. The consequences of the stability of the bow shock surface for its large scale structure are discussed in section 5.2.1.2.

Horbury et al. (2002) also compared timing-based bow shock normal estimates with magnetic field coplanarity, and found large discrepancies (Figure 5.2, middle panel). Coplanarity is known to be a poor estimator of the shock orientation for nearly perpendicular shocks (those where $\theta_{Bn} \approx 90^\circ$; see, e.g Lepidi et al., 1997). This is a consequence of the up and downstream magnetic field vectors being nearly parallel for nearly perpendicular shocks. The large uncertainty in coplanarity nor-

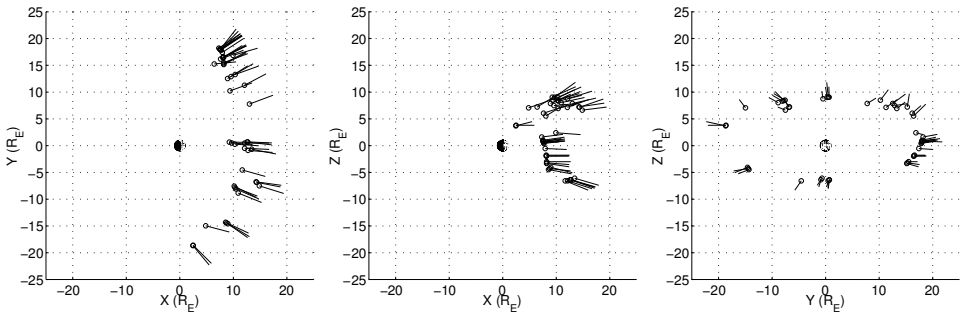

Figure 5.1. Bow shock normals (short lines) deduced from four spacecraft timings, plotted extending from their measured locations (circles). The three panels show the projection of the positions and normals onto the X-Y, X-Z and Y-Z GSE planes. Note that shocks near the nose are not sampled due to the polar Cluster orbit. From Horbury et al. (2002).

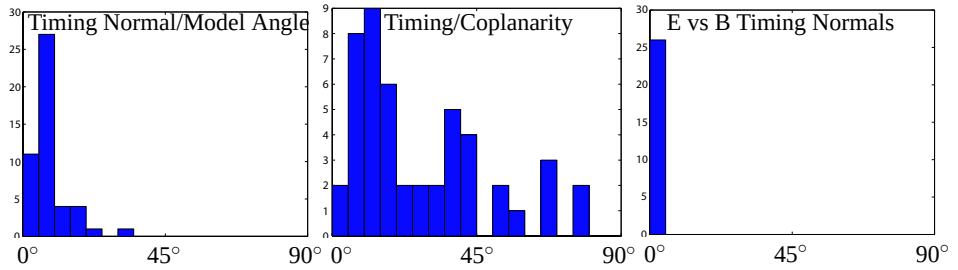

Figure 5.2. Histograms of angular difference between different estimates of quasi-perpendicular bow shock normals. Left: comparison of Cluster four-spacecraft timing normals with normals from a parameterised bow shock model (Peredo et al., 1995). The agreement is good, implying both are typically reliable estimators of the normal. Middle: comparison of timing normals with magnetic field coplanarity. Right: comparison of timing-based normal estimates using magnetic field and spacecraft potential to calculate timings. Left and middle panels from Horbury et al. (2002). Right panel provided by T. S. Horbury and S. D. Bale.

mals for $\theta_{Bn} \approx 90^\circ$, is apparent in Figure 5.3, which shows the deviation of coplanarity vectors from timing-based normal estimates for the shocks considered by Horbury et al. (2002): when $\theta_{Bn} \approx 90^\circ$, the scatter is very large. However, Horbury et al. found that deviations were still large (on average $22^\circ \pm 4^\circ$) for shocks with $\theta_{Bn} < 90^\circ$. This implies that coplanarity estimates of shock orientation can have significant errors even for moderate θ_{Bn} and they must therefore be treated with caution when using single spacecraft data. This is an example of how Cluster multi-spacecraft analysis can help us to interpret other, single spacecraft, data sets.

Horbury et al. (2002) used magnetic field profiles to estimate the shock crossing time at the Cluster spacecraft. However, other parameters can be used: for example, Maksimovic et al. (2003) and Bale et al. (2003) used the spacecraft potential, a

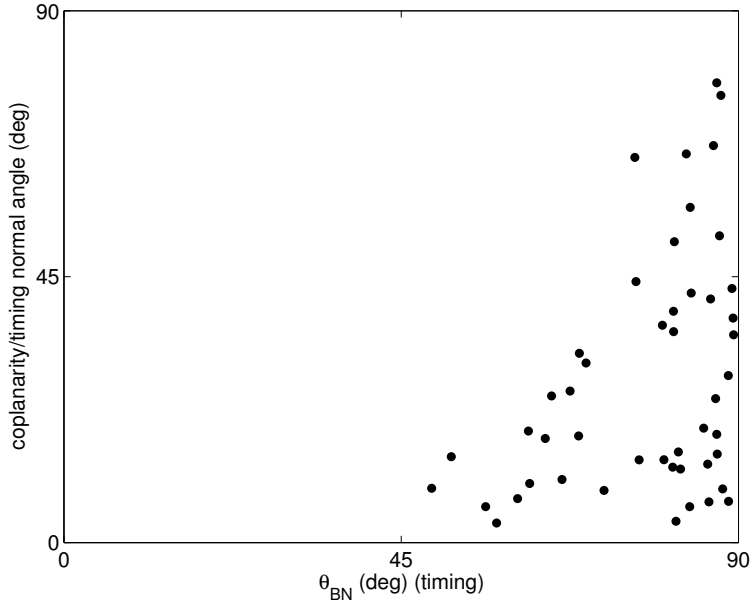

Figure 5.3. Angle between coplanarity and four spacecraft timing estimates of bow shock normals, as a function of θ_{Bn}. Coplanarity is an unreliable estimator of bow shock orientation for $\theta_{Bn} \gtrsim 70^\circ$ but is still only accurate to around 20° for $\theta_{Bn} \lesssim 70^\circ$. From Horbury et al. (2002).

proxy of the local plasma density. It is therefore of interest to compare four spacecraft timing estimates of the shock orientation using these different estimators. We have compared the orientations deduced from EFW (spacecraft potential) and FGM (magnetic field) timings for 26 quasi-perpendicular shocks in 2001 that could be identified cleanly in both EFW and FGM data at all four spacecraft, a subset of those used by Horbury et al. (2002). The agreement between the resulting shock normals is remarkable (Figure 5.2, right panel), with the mean angular deviation being 1.8° and the largest deviation being only 3.9°. The mean absolute difference in the deduced velocity was 2 km/s. While this comparison cannot tell us about the reliability of some of the assumptions (such as constant motion and planarity) of the timing method for quasi-perpendicular shocks, it confirms that it is not sensitive to the physical parameter used.

5.2.1.2 Large scale structure of the bow shock

As discussed above in section 5.2.1.1, Horbury et al. (2002) found close agreement between bow shock normal estimates based on four spacecraft timings and those of bow shock models such as that of Peredo et al. (1995). This implies that the bow shock stays close to the parabolic shape of the Peredo et al. model, at least under

steady solar wind conditions. It also places an upper limit on the size of any large scale 'ripples' on this surface: if they were present to a significant degree, the local normals deduced from the Cluster measurements would not agree with the normal derived from the model normal.

Bow shock models have been derived in the past by estimating the parameters of a conic section from thousands of single spacecraft shock crossing locations, parameterised by upstream conditions such as ram pressure and magnetic field direction. It is therefore remarkable that these models of the large scale shape agree so closely with the local normal estimates from Cluster found by Horbury et al. (2002).

5.2.2 Large- and meso-scale shock structure

5.2.2.1 Dissipation at quasi-perpendicular shocks

Fast-mode collisionless shocks grow from magnetosonic waves when the incoming flow exceeds the fast magnetosonic speed; the wave steepens and eventually becomes a standing shock in the plasma. To stand as a steady-state shock, the plasma must dissipate small-scale structure to slow the steepening and prevent the shock from overturning; furthermore, the Rankine-Hugoniot (shock jump) relations tell us that the shock must convert incoming flow energy to electron and ion heating and magnetic field energy downstream. Early theories of energy dissipation at shocks sought a single mechanism to directly provide both small-scale dissipation *and* plasma heating (viz., Papadopoulos, 1985). Ion and electron heating mechanisms appear to be mostly unrelated.

At quasi-perpendicular collisionless shocks above a critical Mach number (Kennel et al., 1985), a significant fraction of incident ions are reflected within the shock transition. They gyrate in the upstream region, where the magnetic field is slightly increased to form a 'foot' before returning to the steep ramp region. Having gained energy due to the solar wind $\mathbf{v} \times \mathbf{B}$ electric field, they traverse the ramp and become temporarily trapped in the adjacent overshoot region (Paschmann et al., 1982; Sckopke et al., 1983; Sckopke et al., 1990). The ions ultimately convect further downstream, leading to a magnetic undershoot and series of decreasing oscillations accompanied by ion mixing and thermalisation.

The spatial scales over which the shock dissipates energy, and slows the incoming flow, are thought to be related to the nature of the dissipation mechanism itself. Hence, knowing these scales and their dependence on macroscopic plasma parameters is tantamount to knowing the dissipation physics at the shock. Quasi-perpendicular ($Q_\perp$) shocks have been traditionally targeted for dissipation scale studies, including aspects such as:

1. the role/interpretation of competing dissipation mechanisms within more classical frameworks (anomalous resistivity, viscosity, Hall physics)

2. differing scales for the transition of different bulk parameters (magnetic field, density, velocity)
3. Ohm's law, including contributions from electron inertia and departures from isotropy
4. the role of stationary (DC) fields in the dissipation processes (electron kinetics, ion reflection)
5. the role of non-stationary fields in scattering and shaping the particle distributions at, and downstream of, the main shock transition.
6. the competition between dissipation and dispersion in effecting and limiting the steepening of the shock profile.

5.2.2.2 Shock ramp scales

The shock ramp is the region of steepest spatial gradients. The steepening is limited and balanced by dispersion and/or dissipation. The nature of the dissipation differs according to the strength of the shock, i.e. low or high value of the Mach number (Alfvénic M_A or magnetosonic M_{ms}). Resistive dissipation alone is enough at low Mach number, while an additional dissipation (e.g., viscosity) is required at high Mach number. Low and high M_A (or M_{ms}) correspond to subcritical and supercritical Mach regime defined below and above a certain threshold (Tsurutani and Stone, 1985). This balance will define the width of the shock front and in particular the ramp width.

Theoretical and kinetic simulations (Leroy et al., 1982) suggested, together with previous observations, that the magnetic ramp occurs on either an ion inertial scale (c/ω_{pi}) or the gyro-radius of an ion moving at the upstream flow velocity in the downstream magnetic field. While the plasma density tends to follow the magnetic field (Scudder et al., 1986), the electric field shows fine scale features discussed in more detail in Section 5.2.3.

As a multi-spacecraft mission, Cluster was designed precisely to measure spatial scales in the magnetosphere. Typical Cluster spacecraft separations are 100-1000 km which correspond to crossing times of 1-100 s for boundary (shock) speeds of 10-100 km s^{-1}. Hence, sample speeds of 1-10 samples per second are sufficient to sample the shock transition and find a spatial transformation by the techniques discussed above and elsewhere (e.g., Paschmann and Daly (eds.), 1998).

Bale et al. (2003) used the Cluster EFW spacecraft potential as a proxy for electron density to study the ramp transition scale at approximately 100 Q$_\perp$ bow shock crossings. A shock speed (and normal) was found using the timing technique and then each shock profile was fitted with a hyperbolic tangent function $n(x) = n_0 + n_1 \tanh(x/\chi)$. Figure 5.4 shows an example fit at a $M_{ms} \approx 3.5$, $\theta_{Bn} \approx 81^\circ$ shock.

A characteristic scale size for the shock ramp was then given to be $L = n/|dn/dx|$ evaluated at the middle of the ramp and this was expressed in terms of the fit coef-

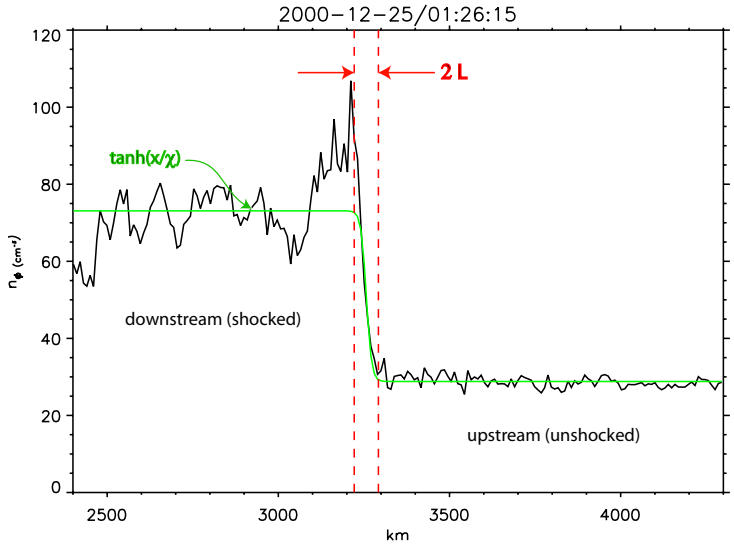

Figure 5.4. Density transition from downstream (shocked) to upstream (unshocked) states for a Mach $M_{ms} \approx 3.5$, $\theta_{Bn} \approx 81^\circ$ shock. The green line is the hyperbolic tangent fit; red vertical lines show the density transition scale. From Bale et al. (2003).

ficients $L = n_0/n_1\ \chi$. Bale et al. (2003) then showed that statistically the measured ramp scale size was proportional to $v_{sh}/\Omega_{ci,2}$, the gyroradius of trapped ions, over a large range of Mach numbers. When compared with the ion inertial scale, $L/c/\omega_{pi}$ is seen to increase monotonically. This is the expected behaviour if the true shock ramp scale is like $v_{sh}/\Omega_{ci,2}$, since $v_{sh}/\Omega_{ci,2}/c/\omega_{pi} \propto M_A$. Figure 5.5 shows these trends.

Similar, supporting results (Horbury, 2004, unpublished) have been obtained using magnetic field data. Taken together, these scalings strongly suggest that the density, magnetic field, and velocity transition scales of the quasi-perpendicular shock are proportional to the gyroradius of the trapped ion population. At low Mach numbers, the two scales $v_{sh}/\Omega_{ci,2}$ and c/ω_{pi} are of similar magnitude and some ambiguity remains. However, the implication of this result is that dissipation at $Q_\perp$ shocks is related to the motion of the trapped ions. In a fluid sense, this corresponds to a viscosity term in Ohm's law associated with gradients in the ion pressure tensor as discussed above.

5.2.2.3 Overshoot/Undershoot structure

It is well known that supercritical shocks exhibit overshoot and undershoot behaviour of the magnetic field just downstream of the shock (Heppner et al., 1967; Russell and Greenstadt, 1979). Since this structure is only observed at supercriti-

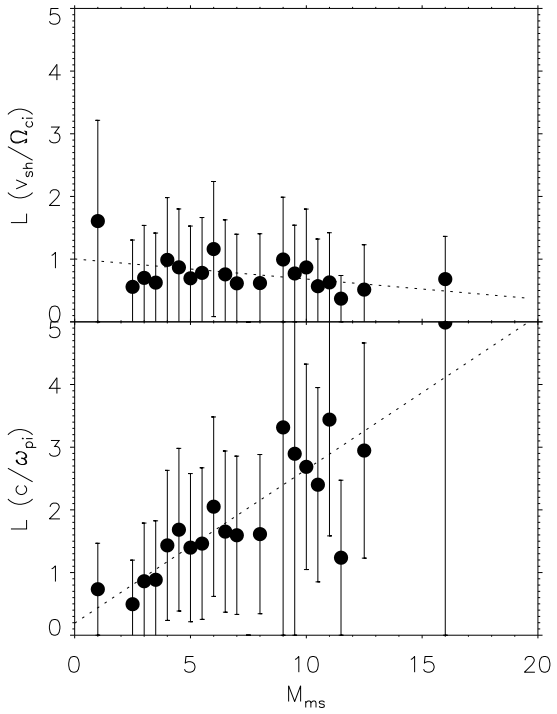

Figure 5.5. Relationship between scale size and magnetosonic Mach number. $L/(v_{sh,n}/\Omega_{ci,2})$ (upper panel) is approximately constant over a large range of Mach number, while the ion inertial scaling (lower panel) increases with Mach number. From Bale et al. (2003).

cal shocks, it was suggested (Morse, 1976) and confirmed by computer simulation (Leroy et al., 1982) that the overshoot structure is associated with a reflected and heated ion population. It is also known that overshoot phenomena play a role in ion acceleration (Giacalone et al., 1991) and electron heating (Gedalin and Griv, 1999). ISEE-1 and -2 measured magnetic overshoot thicknesses using two-point timing to obtain shock speed (Livesey et al., 1982) and found that the observed thickness was ordered by the downstream ion gyroradius. However, Cluster has made the first density measurements of well-defined overshoot-undershoot structure at $Q_\perp$ shocks (Saxena et al., 2004). Using Cluster EFW spacecraft potential as a density proxy, 56 $Q_\perp$ shocks have been analysed using techniques similar to those of Bale et al. (2003).

Figure 5.6 shows typical overshoot/undershoot structure at the same $M_{ms} \approx 3.5$, $Q_\perp$ shock as Figure 5.4. Subtracting the fitted hyperbolic tangent (top panel) leaves a clear 'chirp' signature associated with the overshoot/undershoot (middle panel).

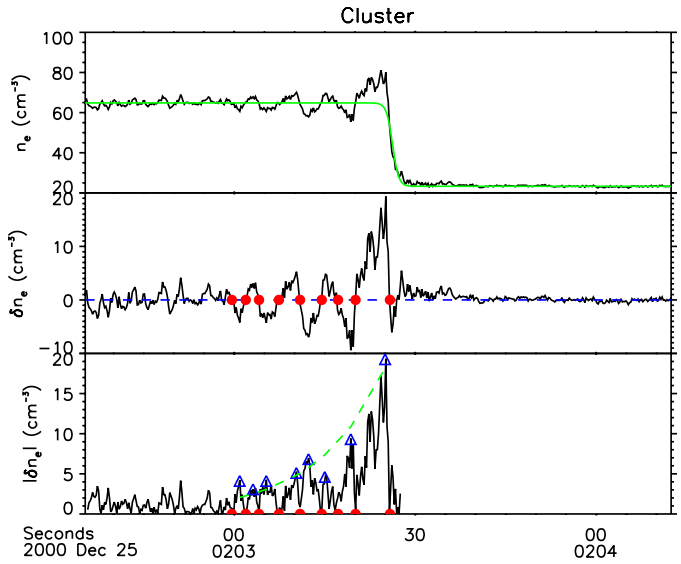

Figure 5.6. Overshoot/undershoot structure at the shock of Figure 5.4 The hyperbolic tangent trend is removed to show a 'chirp' (middle panel); red dots show the location of zero-crossings that are used to measure the overshoot wavelength. The maximum density perturbation between zero-crossings decays spatially (lower panel); blue diamonds show the maxima which are fitted to an exponential to retrieve a decay scale. From Saxena et al. (2004).

Then a zero-crossing algorithm is applied to the chirp (red dots, middle panel) to produce an estimated wavelength for the shock overshoot. Finally, the overshoot amplitude is seen to decay systematically (bottom panel). An exponential function is fitted to the maxima of $|\delta n|$ between each pair of zero-crossings (blue diamonds) to estimate a decay scale λ. *Both* the overshoot/undershoot wavelength and decay scale are found to be organised by the gyroradius of trapped ions, $v_{sh}/\Omega_{ci,2}$, (rather than the ion inertial length). The measured wavelength is consistent with ISEE magnetic observations, while the measurement of an overshoot exponential decay scale is a new result for Cluster.

5.2.3 Fine-scale features in the electric field

Within a collisionless shock front, energy transfer is achieved through the interaction between electric/magnetic waves and particles rather than the normal collisional processes that occur within common hydrodynamic shocks. The spatial scales over which these particles and fields can interact is important when trying to ascertain the energy transfer processes that may occur within the shock front. The determination of magnetic field structure and the spatial scales over which the field

varies in the foot, ramp, and overshoot/undershoot regions has been intensively studied since shocks were first observed in the 1960's.

Typically, the foot width is of the order of $0.68V_{sw}/\Omega_{ci}$ where V_{sw} is the solar wind velocity and Ω_{ci} is the upstream ion gyrofrequency (Sckopke et al., 1983; Livesey et al., 1984). The ramp scale has been estimated to be less than an ion inertial length (e.g., see Balikhin et al., 1995, and references therein) with reports of one or two shocks whose ramp scale was of the order $0.1c/\omega_{pi}$ (Newbury and Russell, 1996; Walker et al., 1999). Figure 5.5 shows, however, that at larger Mach numbers the shock ramp is typically larger than an ion inertial length.

Reports of observations of the electric field, on the other hand, are very sparse. This was probably due to the lack of high quality, high time resolution measurements. Based on initial results from ISEE, Heppner et al. (1978) reported that short duration spike-like features were occasionally observed in the electric field as the satellite crossed the shock front. Further investigations of subcritical oblique shocks by Wygant et al. (1987) showed spike-like features with amplitudes up to $100\,\mathrm{mV\,m^{-1}}$ and a strong component along the shock normal. The observations were, however, not good enough to determine the free energy source, mode or scale size of these structures. They speculated that these waves may be either lower-hybrid or possibly Doppler shifted ion-acoustic waves. Based on spin averaged electric field measurements from ISEE, Formisano (1982) reported that the increase in the electric field observed at quasi-perpendicular shocks began just upstream of the magnetic ramp and lasted longer than the ramp crossing itself.

One key aspect to determine is the spatial scale over which changes in the electric field occur and its relation to the scale size over which changes in the magnetic field occur. Several differing points of view have been published. The first (Eselevich et al., 1971; Balikhin et al., 1993; Formisano and Torbert, 1982; Formisano, 1982, 1985; Balikhin et al., 2002; Krasnosel'skikh, 1985; Leroy et al., 1982; Liewer et al., 1991; Scholer et al., 2003) is that the spatial scales of the potential and magnetic field in the ramp region are similar whilst Scudder (1995) proposed the potential scale length is larger than that of the magnetic scale length. Others have suggested that the potential varies predominantly within iso-magnetic jumps, i.e., on a smaller scale than the magnetic field. In laboratory plasmas, such a short scale of the cross-shock electrostatic potential ('isomagnetic jump') was observed by Eselevich (1982). This isomagnetic jump is often attributed to the ion sound subshock (see the review by Kennel et al., 1985).

Using data generated from numerical simulations, Lembège et al. (1999) analysed simultaneous measurements of the scale size of both the magnetic ramp region and the region in which the change in potential was observed. Their results showed that the scale lengths were of the same order. This view is also supported by the simulations of Scholer et al. (2003). The latter authors show that the main potential drop can occur over several ion scales in the foot region, while the steepened

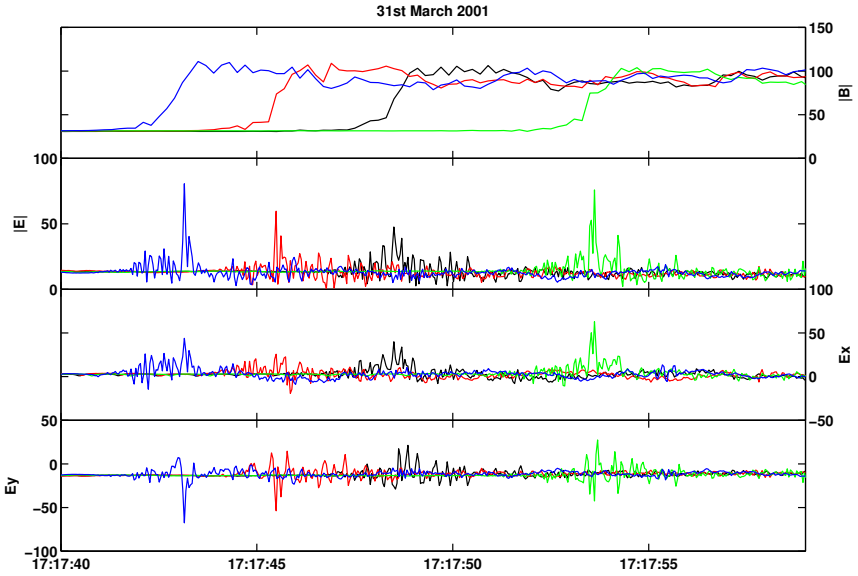

Figure 5.7. Overview of the shock crossing on March 31, 2001 at 1718 UT. The top panel shows the magnitude of the magnetic field measured by FGM. The second panel shows the magnitude of the electric field measured in the satellites' spin plane. The lower two panels show the spin plane components E_x and E_y. The four traces correspond to Cluster 1 (black), 2 (red), 3 (green) and 4 (blue). From Walker et al. (2004).

magnetic ramp region also contributes a significant fraction of the change in total potential over much smaller scales, typically 5-10 electron intertial lengths.

In this section we present the results of an investigation by Walker et al. (2004) into the spatial size of high amplitude, short lived spike like features observed in the electric field during a number of encounters with the quasi-perpendicular terrestrial bow shock. All electric field data presented were collected by the Cluster EFW instruments (Gustafsson et al., 1997), were sampled at 25 Hz, and have an upper cutoff frequency of 10 Hz.

As an example of the type of phenomena being investigated, Figure 5.7 shows an overview of the FGM magnetic field and EFW electric field for the shock encountered on March 31, 2001 at around 17:40 UT. The shocks observed on this particular day are not typical due to the passage of a CME that erupted from the sun a couple of days before. As a result, the upstream parameters were as follows: $|\mathbf{B}| \approx 30$ nT, $\theta_{Bn} \approx 87^\circ$, particle density $n \approx 19\,\mathrm{cm}^{-3}$, and an Alfvén Mach number (M_A)≈ 3.6. The normal for this shock (based upon FGM crossing times) is $n_B = (0.94, -0.17, 0.293)$ (in the GSE frame), and the shock velocity was determined to be $48.92\,\mathrm{km\,s}^{-1}$.

The top panel shows the magnitude of the magnetic field measured by the four Cluster spacecraft. The data show that the satellites crossed the shock at 17:17:43.5 (Cluster 4), 17:17:45.5 (Cluster 2), 17:17:48.5 (Cluster 1), and 17:17:53.5 (Cluster 3). and that the foot, ramp and overshoot regions are clearly identifiable. The second panel shows the magnitude of the electric field measured in the spin planes of the satellites ($|E| = \sqrt{E_x^2 + E_y^2}$). The disturbances in the electric field begin in the magnetic foot region and continue through the overshoot/undershoot region. For this particular shock the field increase is around 6-7 mV m^{-1} when compared with the solar wind in both the foot and overshoot regions. However, in the region of the magnetic ramp the electric field exhibits increases of between 30 and 65 mV m^{-1} lasting a few hundred milliseconds. It is also obvious that the peaks appear in pairs. Inspection of the lower two panels (electric field spin plane components) shows that these peaks correspond to a rotation in field away from the projection of the normal onto the spin plane. By using the timings of the first peak observed in the electric field it is possible to compute a normal direction and velocity. This normal lies within a degree of that determined by FGM, and produces a similar value for the velocity. Thus it appears that these large amplitude, short duration features in the shock front appear to be some form of structured layer within the shock front.

Similar large amplitude, short duration features in the electric field have been observed at a number of shock crossings although their amplitudes are typically 10-20 mV m^{-1} above that observed in the solar wind. Their spatial scale and its variation with respect to the upstream shock parameters have been investigated. Figure 5.8 shows the distribution of scale sizes measured in electron inertial lengths (c/ω_{pe}). This measurement is unaffected by the fact that only two of the three electric field components are measured. It shows that the majority of scale sizes are of the order 1-5 c/ω_{pe}, a value much smaller than that of the magnetic ramp scale reported in Section 5.2.2.2. This measurement also shows that substantial contributions ($\approx 50\%$) to the overall cross shock potential occur within small regions of the shock.

The relationship between the scale size of the electric field spikes and the Alfvén Mach number is shown in Figure 5.9. It would appear that the scale size has an upper limit that increases as the Mach number decreases.

Figure 5.10 shows a scatter plot of the scale size of the electric field enhancements as a function of θ_{Bn}. The range of scale sizes appears to decrease as $\theta_{Bn} \rightarrow 90^\circ$. Karpman (1964) proposed that for shock with $\theta_{Bn} \approx 90^\circ$ the scale lengths are of the order of an electron inertial length. Indeed, although the errors in the determination of θ_{Bn} are probably $\sim 5^\circ$, the most nearly perpendicular Cluster shocks show scale lengths on the order of $2c/\omega_{pe}$.

Analysis of the field increase ($\Delta E = E_{spike} - E_{upstream}$) observed during these events show that their amplitudes vary in the range 4-70 mV m^{-1} above that measured in the solar wind upstream of the shock front. A scatter plot of the variation

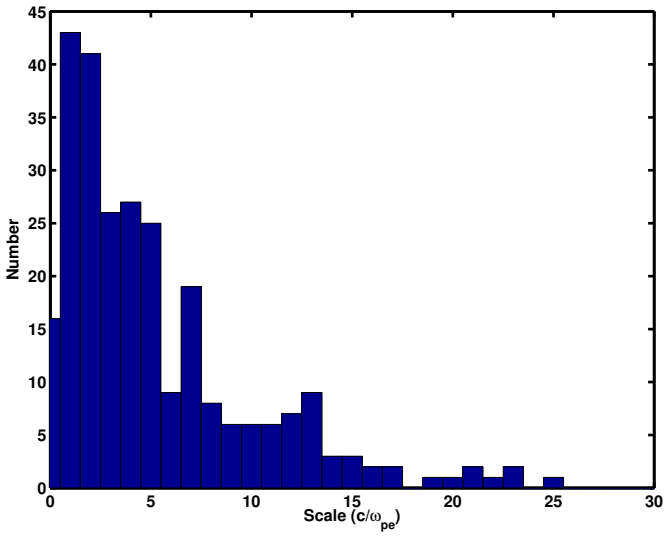

Figure 5.8. A histogram of the scale sizes for the spike-like enhancements observed during a number of crossings of the quasi-perpendicular bow shock. The typical width of a few electron inertial lengths (c/ω_{pe}) is much less than that of the magnetic field and density ramps. From Walker et al. (2004).

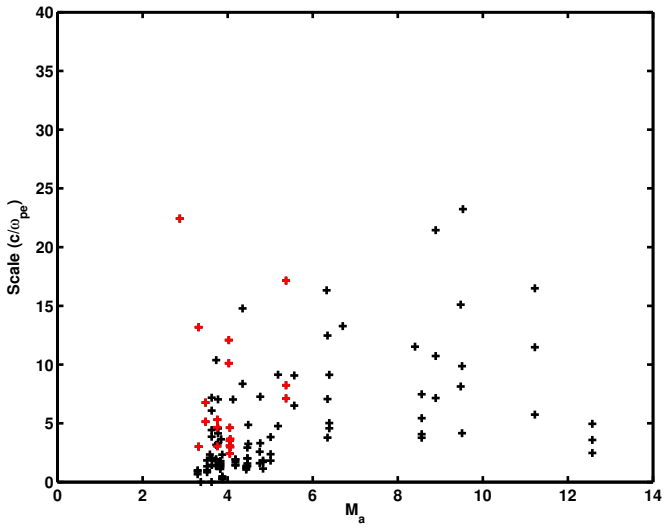

Figure 5.9. The dependence of electric field scale size on upstream Mach number. The red crosses are used to highlight the data for the shocks that occurred on March 31, 2001 under unusual conditions (Balikhin et al., 2002). From Walker et al. (2004).

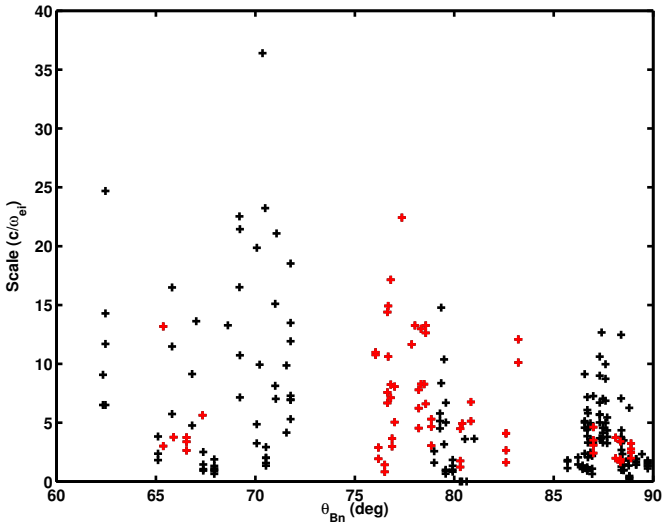

Figure 5.10. The dependence of electric field scale size on θ_{Bn}. From Walker et al. (2004).

of the peak field increase as a function of Mach number is shown in Figure 5.11. It can be seen that for those shocks whose Mach number $M_A > 5$ the value of ΔE is fairly constant and typically $\Delta E < 15$ mV m^{-1}. In contrast, for Mach numbers in the range $3 < M_A < 5$ the electric field amplitudes show a much larger spread, covering a range 5 - 60 mV m^{-1}. The shocks marked by red crosses correspond to those observed on March 31, 2001, a subset of shocks in a particularly interesting range of Mach numbers discussed in detail in Balikhin et al. (2002).

The relationship between ΔE and θ_{Bn} is shown in Figure 5.12. It clearly shows that as $\theta_{Bn} \rightarrow 90^\circ$ the range of the observed amplitudes of the electric field spikes increases.

5.2.4 Shock variability and non-stationarity

5.2.4.1 Introduction

Shock waves in plasmas as well as in gases and other media are nonlinear waves that cause changes of state of the media and are usually considered to be stationary in some reference frame. However, even early work in the subject (Morse et al., 1972) revealed evidence of non-stationarity in laboratory experiments. They revealed that in the fast magnetosonic mode Mach number range $M_{ms} \simeq 4$–8 the shock wave oscillates with a frequency comparable to the upstream ion gyrofrequency. The extent to which the physics of collisionless shocks involves intrinsically non-stationary processes has remained an open question. A compounding problem is the non-steady propagation speed of a shock which leads, for example

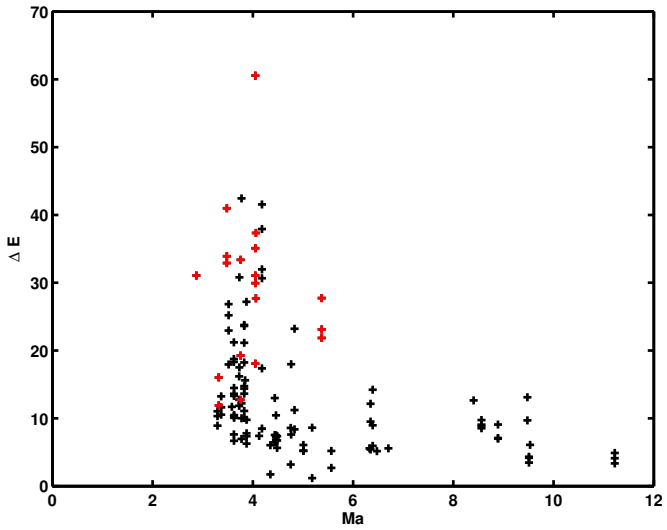

Figure 5.11. Scatter plot showing the relationship between the amplitude of the electric field spikes as a function of Mach number. From Walker et al. (2004).

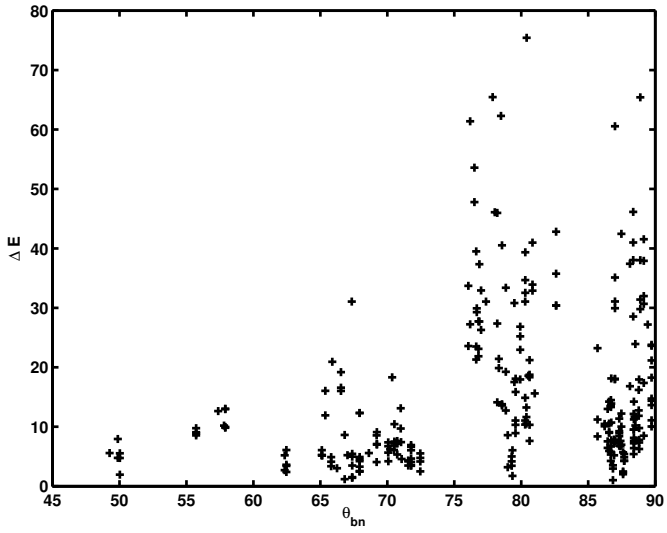

Figure 5.12. The relationship between the amplitude ΔE of the electric field spikes and θ_{Bn}. Shocks closer to 90° show a higher range of amplitudes. From Walker et al. (2004).

in the case of the Earth's bow shock, to relative motion of the bow shock with respect to the Earth in response to changes in solar wind conditions.

In the early 1980s, in the response both to new observations of the Earth's bow shock and computational capabilities, collisionless shock physics matured rapidly (e.g., Kennel et al., 1985, and accompanying papers). Indications of non-stationarity were found in low frequency oscillations of the ion flux at the bow shock (Vaisberg et al., 1984, 1986a,b) and at the bow shock of Uranus (Bagenal et al., 1987). Kinetic hybrid simulations (Leroy et al., 1981, 1982) for parameters typical at the Earth's bow shock ($M_A = 8$ and $\beta_e = \beta_i = 0.6$, where M_A is the Alfvén Mach number, $\beta_{e,i}$ is the ratio of the thermal and magnetic pressures, and 'e' and 'i' refer to electrons and ions respectively) showed that the shock structure varies with time. For example, the maximum value of the magnetic field exhibits temporal variations with a characteristic time of the order of the ion gyroperiod, the magnitude of these variations being about 20%.

Quest (1985) modelled high Mach number perpendicular shocks ($M_A = 22$, $\beta = 0.1$). In the absence of electron resistivity the ion reflection process is periodic, alternating between periods of 100% ion reflection and 100% ion transmission. As a result, a periodic shock front reformation was observed rather than a stationary structure. Quest (1986) extended these preliminary simulations to perform a systematic study of high Mach number perpendicular shocks. For $\beta = 0.1$ he revealed that the previously found (Leroy et al., 1982) tendency of a shock to become increasingly time-dependent as M_A increases was also observed for $M_A \geq 10$ and resulted in cyclical wave breaking for $M_A \geq 20$. In addition, for $\beta = 1$ and $M_A \geq 10$ a non-trivial dependence of the shock front structure on the resistivity was found.

Krasnosel'skikh (1985) and Galeev et al. (1988c) proposed models that attribute the shock front instability to the domination of nonlinear effects over dispersion and dissipation. Non-stationary whistler wave trains, which had been previously suggested (Galeev et al., 1988c,b,a), were reported in observations of the Earth bow shock onboard Intershock-Prognoz-10 and AMPTE UK spacecraft (Krasnosel'skikh et al., 1991). Recently, theoretical work and 1D full particle simulations have been used to analyse this mechanism in detail. Its application to obliquely propagating shocks has revealed a critical Mach number above which these non-stationarity processes operate (Krasnosselskikh et al., 2002).

Lembège and Dawson (1987b) have shown that the non-stationarity of the shock front can be due to the cyclic self-reformation of the shock front, and have recovered fluctuation levels of 20% in the magnetic field at the overshoot amplitude and in the density of reflected ions. They analysed this self-reformation in detail for an exactly perpendicular low-beta non-resistive shock in 1D full particle simulations and showed that this reformation persists even for a moderate (still supercritical) Mach number ($M_A = 2 - 4$). This non-stationary process persists over an angular range below $\theta_{Bn} = 90^\circ$ as long as the density of reflected ions is high enough to feed the reformation (Lembège and Dawson, 1987a). Lembège and Savoini (1992) confirmed the previous results with the help of 2D full particle simulations and showed that reformation continues to occur even when finite resistivity effects due to cross

field current instabilities are included self-consistently. In addition, the shock front appears to be rippled rather than uniform for both perpendicular and oblique planar shocks. Moreover, the reformation is expected for relatively low ion β_i (i.e. relatively cold upstream plasma) and/or high Mach number shocks, but disappears as β_i reaches relatively high values as shown by both 1D hybrid (Hellinger et al., 2002) and 1D full particle simulations (Scholer et al., 2003; Hada et al., 2003).

The problem of shock front stationarity described above gives several indications about possible manifestations of these effects in observations. Most of the results indicate that the characteristic timescale of the shock front variations is of the order of one ion gyroperiod or less, related to either the physics of the whistler mode expected to dominate the overall transition and/or the overturning due to nonsteady ion reflection. This time period is comparable to and often shorter than that required to obtain full ion and electron distributions by Cluster. As noted above, shock motion can complicate this matter. Indeed, most of what we know about the position and shape of the bow shock is based on statistical studies together with modelling (e.g., Peredo et al., 1995, and references therein); the detailed response of the bow shock position to fluctuations in the upstream solar wind conditions has not been practical prior to the multi-spacecraft approach of Cluster.

In the following sections we provide an overview of the key Cluster results in this area. Evidence for intrinsic non-stationarity comes by studying variations of the shock profile, and by inferences on the variability of the ion reflection process(es). Cluster has also addressed directly the motion of the bow shock.

5.2.4.2 Shock profile variability

The near-simultaneous measurement of the shock profile by four spacecraft allows us to study spatial and temporal variability in ways that have not previously been possible. Different physical parameters such as the density, electric field and magnetic field would be expected to vary in different ways. The variability of one of these, the magnetic field, through the quasi-perpendicular shock was considered briefly by Horbury et al. (2001).

By considering the magnetic field profile through a nearly perpendicular supercritical shock ($\theta_{Bn} \approx 86^\circ$, plasma $\beta \approx 0.1$, Alfvén Mach number $M_A \approx 4.8$), Horbury et al. (2001) could identify structures which were stationary (i.e., phase standing) relative to the main shock ramp, and others that were not. The shock is shown in the top panel of Figure 5.13: the four profiles look superficially very similar. When the profiles are synchronised at the time of the crossing (Figure 5.13, bottom panel), some other features become visible. In particular, the shock overshoot, undershoot and subsequent oscillations in the magnetic field magnitude are fairly well synchronised between the four spacecraft, implying that this field magnitude structure does not vary significantly over the spacecraft separation (around 600 km) or the time differences between the shock passages of the different spacecraft (up to 30s).

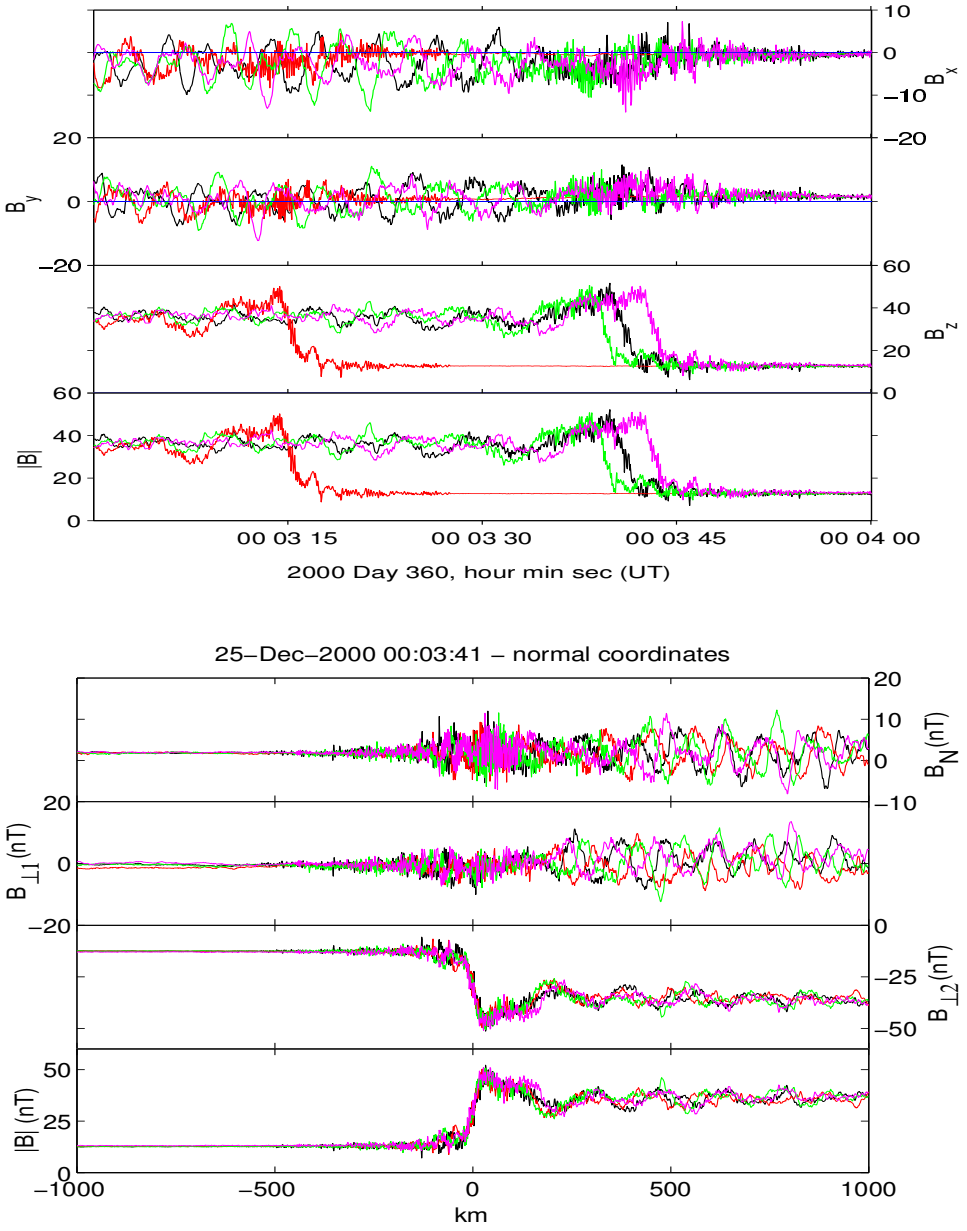

Figure 5.13. A supercritical quasi-perpendicular shock encountered by the Cluster spacecraft. Top: magnetic field data in GSE coordinates. Data from all four spacecraft are shown in different colours. Bottom: the same data, synchronised at the shock transition and transformed into a spatial scale and a shock-aligned coordinate system. The downstream oscillations in the field magnitude are well synchronised between the spacecraft, while the downstream field-perpendicular waves are not, implying that the latter are not phase standing with respect to the shock front. From Horbury et al. (2001).

In contrast to the shock profile in the magnetic field magnitude, the downstream large amplitude waves (with a polarisation and frequency consistent with ion cyclotron waves generated by non-gyrotropic ion distributions) varied significantly between spacecraft, confirming that these waves were not stationary with respect to the shock transition - again, this is clear from the synchronised profiles in Figure 5.13. In addition, it was not possible to identify the same waves at different spacecraft, implying that the scale sizes of these waves along the shock front were not larger than the spacecraft separations of around 600 km - their wavelength along the shock front was around 100 km. Analysis of shocks when the spacecraft are closer together will make it possible to identify the same wave at different spacecraft, and unambiguously determine the wavelength, propagation direction and speed of the downstream waves. There were also high frequency waves around the shock foot and ramp, which were consistent with whistlers.

Unlike the shock shown in Figure 5.13, which exhibits a rather steady background profile, Horbury et al. (2001) also considered a shock with a varying profile (Figure 5.14). The parameters of this shock were $\theta_{Bn} \approx 89^\circ$ and $M_A \approx 5.6$. Here, significant differences are visible in the magnetic field profile measured by different spacecraft - for example, at spacecraft 3 (shown in green in Figure 5.14) the magnetic field magnitude actually decreases from its upstream value before increasing up the ramp, which is not the case at any of the other three spacecraft.

To study this variability in more detail, Horbury et al. (2001) synchronised the four shock profiles (in the same way as the right panel of Figure 5.13), calculated the average profile, and the deviations from the average at each of the four spacecraft; both are shown in Figure 5.15. The average profile exhibits a foot - an increase in the field magnitude before the main ramp - despite this not being clear in any of the four individual profiles in Figure 5.14. This highlights the difficulties of analysing shocks with single spacecraft: it is extremely difficult to determine which features are variable, and which are steady. With four profiles, however, we can begin to distinguish these effects.

The variability of the foot profile is clear in the right panel of Figure 5.15, which shows the deviation of the shock measured at each spacecraft from the average shown in the left panel. Deviations are apparent in the shock foot, but they are not present in the ramp. This implies that the fluctuations in the foot do not propagate into the ramp, and therefore cannot be a source for downstream waves. Horbury et al. (2001) noted that these may be signatures of unsteady reformation (Lembège and Savoini, 1992). The polarisation of these fluctuations – left-handed with respect to the magnetic field in the spacecraft frame - is consistent with whistler, but not Alfvén, waves. The large differences in the foot profile at the different spacecraft, even though the measurements are less than 10 s and 1000 km apart, show the small spatial or temporal scales of these fluctuations.

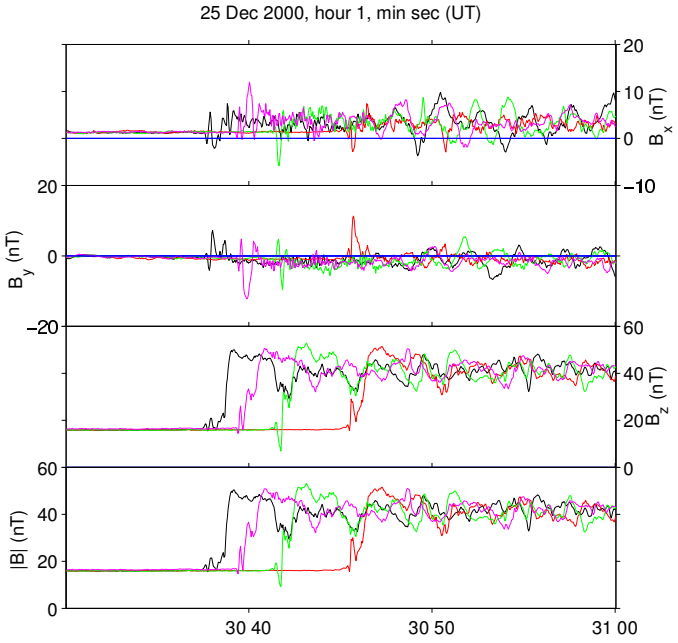

Figure 5.14. A quasi-perpendicular shock with a non-steady magnetic field profile. Clear differences between the profiles at different spacecraft are visible at the beginning of the magnetic field increase of the shock. From Horbury et al. (2001).

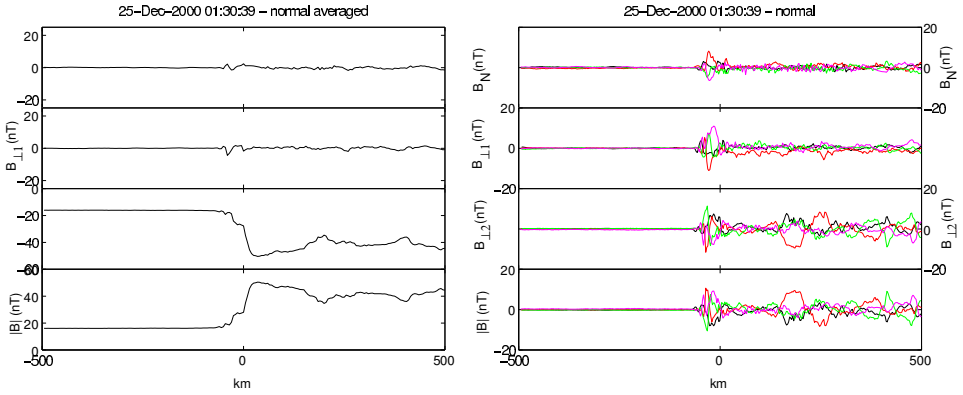

Figure 5.15. Left: Magnetic field profile of the shock shown in Figure 5.14, averaged over the four Cluster spacecraft in shock normal coordinates. A foot is clearly visible. Right: deviations of the magnetic field profile at each spacecraft from the average shown in the left panel. Variations are apparent in the foot, but not the ramp, demonstrating that the foot profile is variable, but that these fluctuations do not propagate into the shock ramp. From Horbury et al. (2001).

5.2.4.3 Variability of particle distribution functions

The bow shock is nearly always supercritical, so that the required heating cannot be accomplished purely resistively. The primary ion heating mechanism involves the reflection of a fraction of the incident ion population, which then gyrate around the magnetic field and return to the shock, thereby spreading the ion population in velocity space (Paschmann et al., 1982; Sckopke et al., 1983). While Cluster observations (Möbius et al., 2001; Kucharek et al., 2004) show that the fluxes of field-aligned beams upstream of the shock can be quite steady, they nonetheless reveal periodic variations by a factor ~ 3 (see Section 5.3.1.3). Closer to the shock the flux of reflected ions is modulated in response to changes in the local shock geometry (Meziane et al., 2004). This topic is addressed more completely in Eastwood et al. (2005, this issue). Identifying the signatures of particle variations associated with intrinsic shock front non-stationarity is more challenging since the spin period of the spacecraft, which limits the time resolution of the particle populations, is comparable to the relevant ion timescales.

5.2.4.4 Bow shock motion

In addition to variability of the shock front structure, the shock itself is in constant motion. It is important to be able to distinguish shock front variability from acceleration and motion in spacecraft data. Shock motion itself is also a topic of interest: changes in upstream conditions can alter the equilibrium position of the shock, but it is apparent that the shock moves even when the incoming solar wind is very steady. The shock motion, especially its acceleration, provides insight into the dynamics of its role in slowing the incident solar wind, and hence on the aspects of the shock which affect the global solar wind-magnetospheric interaction. Four spacecraft Cluster data can help us to measure this acceleration with far more confidence than estimates based on single spacecraft measurements.

Some crossings of the bow shock by Cluster show significantly different profiles at the four spacecraft. While these differences can reflect genuine temporal variability in the shock, for example due to reformation (see Section 5.2.4.1) or a change in upstream conditions, they can also be the result of changes in the speed of the shock. Shock crossings consistent with such acceleration - with profiles at some spacecraft significantly compressed or expanded in time compared to others, but otherwise similar - are relatively common in the Cluster data set. As ever, the spacecraft separation is important: at the smallest Cluster separations (around 100 km), where the times between crossings are at most a few seconds, evidence of acceleration is less common than at 5000 km separations, where there is more time between crossings for the shock to change speed.

Dunlop et al. (2002) used the ‘discontinuity analyzer’ (Dunlop and Woodward, 1998) to study the acceleration of the quasi-perpendicular bow shock. The discontinuity analyzer procedure requires an independent method to determine the shock orientation. Then, by determining the relative times at which pairs of spacecraft

encountered the shock, the average speed of the shock between the two points can be estimated. Finally, by considering how this speed changes between successive pairs of spacecraft, the acceleration of the shock can be estimated.

Dunlop et al. (2002) used both coplanarity and minimum variance estimates of bow shock orientations, and found that they were consistent and close to model normals, and therefore were likely to be reliable estimators of the shock normal. They considered quasi-perpendicular bow shock crossings at ≈600 km spacecraft separations and showed that there was evidence of considerable deceleration of the shock transition - in one case, from 147 km s^{-1} to 27 km s^{-1} in around 10 s. This deceleration was usually smooth from one spacecraft to another, although sometimes it was more variable.

Maksimovic et al. (2003) used Cluster measurements of eleven quasi-perpendicular bow shocks on March 31, 2001 to measure the speed and location of the shock, and therefore estimate its large scale motion over more than two hours. They used simple four spacecraft timings, assuming planarity and constant motion during each shock crossing. On the basis of the shock location and orientation and a parabolic model of the shock surface, they could estimate the distance to the shock at the nose, i.e., the sub-solar distance. Using the measured shock speed, they then estimated the instantaneous speed of this sub-solar point, and interpolated it for times between the measured crossings using a cubic polynomial (Figure 5.16, panel a). For one pair of shock crossings, only one of the four spacecraft encountered the shock, so Maksimovic et al. (2003) assumed that it reversed its motion at that location and time.

A number of models have been developed that relate the bow shock sub-solar distance to upstream conditions such as the solar wind ram pressure. Many of these models are based on gas dynamic simulations by Spreiter et al. (1966). Maksimovic et al. (2003) used a combination of the Farris and Russell (1994) and Sibeck et al. (1991) models, with a dependence of the sub-solar distance a_s (in R_E) on solar wind ram pressure P (in nPa) and Alfvén Mach number M_A that scaled as

$$a_s = 12.2 \left(\frac{2}{P}\right)^{1/6} \left[1 + 1.1 \frac{(\gamma-1)M_A^2 + 2}{(\gamma+1)(M_A^2-1)}\right] \tag{5.1}$$

Maksimovic et al. (2003) used ACE data for upstream solar wind and magnetic field conditions, estimated the sub-solar distance and compared it with their estimates based on the Cluster crossings (Figure 5.16, panel b). The agreement was reasonably good, both in absolute position at various times, and in the amplitude of the variations in sub-solar distance (around 6 R_E from the Cluster observations, and 4-5 R_E from the model), implying that the model is valid not only in a statistical sense but also on shorter timescales as the shock responds to changing upstream conditions. Maksimovic et al. (2003) pointed out that their study could be refined further, allowing for effects such as changes in solar wind magnetic field, relative

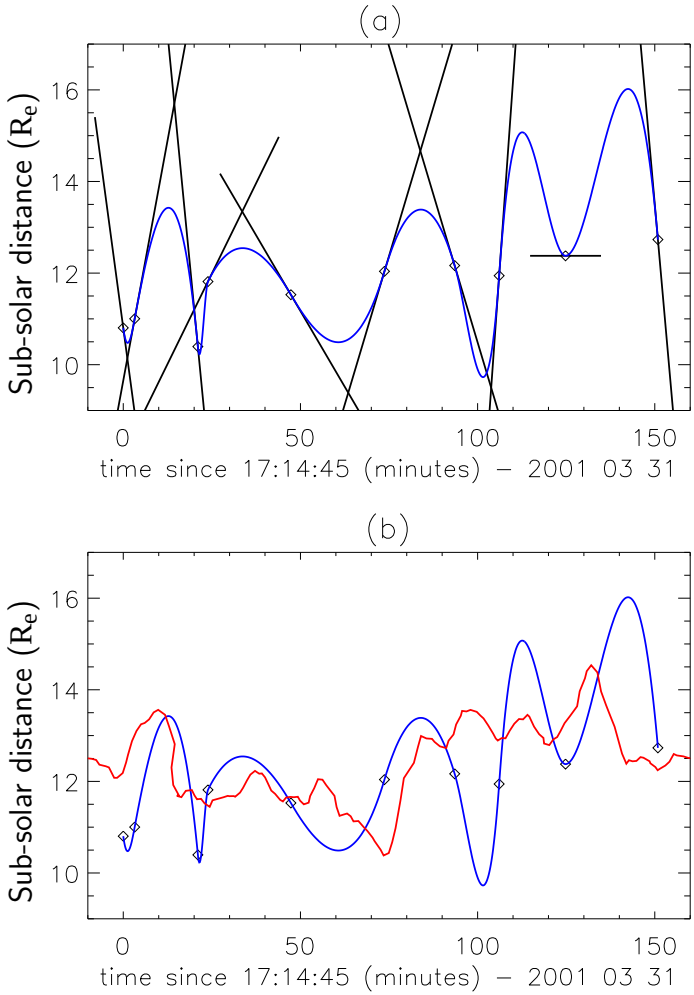

Figure 5.16. Motion of the bow shock sub-solar distance deduced from the measured location and speed of the shock at Cluster. Panel a: Sub-solar distance deduced from individual crossings (diamonds), and extrapolated from the estimated shock speed (black lines). The blue line shows a cubic interpolation through these points, allowing for the measured speeds. Panel b: Deduced sub-solar position in blue, as panel a, compared with the position calculated from a gas dynamic model using upstream solar wind parameters as input (red line). From Maksimovic et al. (2003).

propagation delays between ACE and the bow shock, and local measurement of shock acceleration from the Cluster formation.

5.3 On the formation and origin of field-aligned ion beams

5.3.1 Ion distributions at the quasi-perpendicular bow shock

A very prominent feature at the Earth's bow shock is the presence of backstreaming ions (Asbridge et al., 1968; Lin et al., 1974). The properties and morphology of these ion populations have been intensively studied over the past 30 years using in situ spacecraft observations. With the International Sun Earth Explorer (ISEE) spacecraft substantial progress was made with detailed observations in the foreshock region. This work resulted in the discovery of the different types of upstream distributions depending on the orientation of the magnetic field at the shock (Gosling et al., 1978; Bame et al., 1980; Greenstadt et al., 1980; Paschmann et al., 1981). A very collimated ion beam is found upstream of the quasi-perpendicular shock, and reflected gyrating ions are seen within one gyro-radius of the shock front.

Over the past 15 years the combination of computer simulations and detailed spacecraft observations has improved our knowledge of the processes at the bow shock as a prime example for collisionless shocks considerably. Although significant progress has been achieved in understanding the global dynamics of the ion distributions in the foreshock region, the underlying production mechanisms are still largely unexplained, and models may sometimes even be contradictory to observations. The origin and the basic production mechanism of field-aligned ion beams is such an example.

5.3.1.1 Characteristics of field-aligned beams

ISEE observations have provided well-documented characteristics of field-aligned ion beams, with most of them observed at $\theta_{Bn} < 70^o$. Studies by Paschmann et al. (1981) and Bonifazi and Moreno (1981) suggested that the characteristics of these beams are largely independent of θ_{Bn}. Typically they show an average flow speed which is on the order of twice the solar wind speed, but sometimes it can be significantly higher. Their density reaches up to about 1% of the solar wind, but it can be much smaller. Paschmann et al. (1981) found that these beams consistently exhibit a temperature anisotropy ($T_\perp/T_{||} \approx$ 4-9), where $T_\perp$ and $T_{||}$ are the temperatures perpendicular and parallel to the magnetic field. The perpendicular temperature is usually much larger than the solar wind temperature, which is in the keV range. Beams at larger shock normal angles ($\theta_{Bn} > 70^\circ$) have been observed reaching much higher energies. Their bulk speed was higher by a factor of 5 (or even larger) than the solar wind bulk flow. Usually, these beams show a consistently higher temperature anisotropy.

Although previous observations have documented the characteristics of the upstream ion distributions rather well, they have not been sufficient to determine the source and production mechanism of the ion beams. Multi-spacecraft missions, such as Cluster, are bound to improve our understanding substantially, as they pro-

vide simultaneous observations at different locations and thus unravel temporal and spatial variations, even in 3 dimensions. Simultaneous observations upstream and downstream and/or in the shock ramp allow decisive tests on proposed sources.

5.3.1.2 Characteristics of reflected gyrating ions

In contrast to field-aligned beams, under quasi-perpendicular shock geometries gyrating ions only occur immediately in front of the shock and do not really escape upstream. The maximum of this distribution is seen at a specific pitch-angle that is determined by the orientation of the shock normal relative to the IMF and the solar wind direction. From detailed observations with ISEE-1 and -2 a firm picture of the evolution of these ions has developed.

A small percentage of the incoming protons is specularly reflected. During their gyration in the upstream magnetic field they gain energy by their motion parallel to the convection electric field of the solar wind. They subsequently encounter the shock and are transmitted downstream, where they constitute a gyro-phase bunched distribution (Sckopke et al., 1983; Sckopke et al., 1990). This gyro-phase bunched distribution develops into a ring in velocity space and, through interaction with the directly transmitted solar wind protons, into a pancake-like distribution. The large $T_{\perp}$ vs. $T_{||}$ anisotropy excites Alfvén ion cyclotron and/or mirror waves which, by pitch angle scattering, further downstream lead to the final hot magnetosheath distribution. In other words, specular reflection, gyration, wave excitation, and isotropization of the ions is essential for the formation of the hot magnetosheath flow and provides the mechanism for dissipation of bulk energy at the quasi-perpendicular shock.

In the past this reflected gyrating ion distribution has been distinguished from the field-aligned beam distribution (e.g., Gosling and Robson, 1985; Thomsen, 1985). While the specular reflection of the gyrating ring distribution has been explained in a straight-forward manner as a reflection by the shock potential, for specific phases of the incoming ions and assisted by gyro-motion in the compressed IMF downstream of the shock, the generation of the beam was not so readily understood.

5.3.1.3 Cluster observations of ion distributions upstream of the quasi-perpendicular bow shock

Recent Cluster results show that the ion beam distribution is closely related to the gyrating ion distribution formed by specularly reflected ions (Möbius et al., 2001). In their work, CODIF and HIA data of the CIS instrument were used to study the time evolution of the velocity distribution of reflected ions during a time period of repetitive shock crossings of the Cluster spacecraft. There is clear evidence that the gyrating and beam distributions are intimately connected. In fact, the beam distribution that escapes from the shock along the magnetic field lines emerges from the low pitch-angle wing of the specularly reflected ion distribution in the shock ramp under flux conservation.

The key results from this study are illustrated in Fig. 5.17. Shown are full sky maps of the H^+ distributions at 2.2 – 3.5 keV for four time periods on the left and the magnetic field strength on all 4 spacecraft as well as ion fluxes for the gyrating ions from Cluster 4 and the beam from Cluster 1, 3, and 4 as a function of time on the right. The ramp location is indicated in the figure for Cluster 1 as are the times corresponding to the displayed angular distributions.

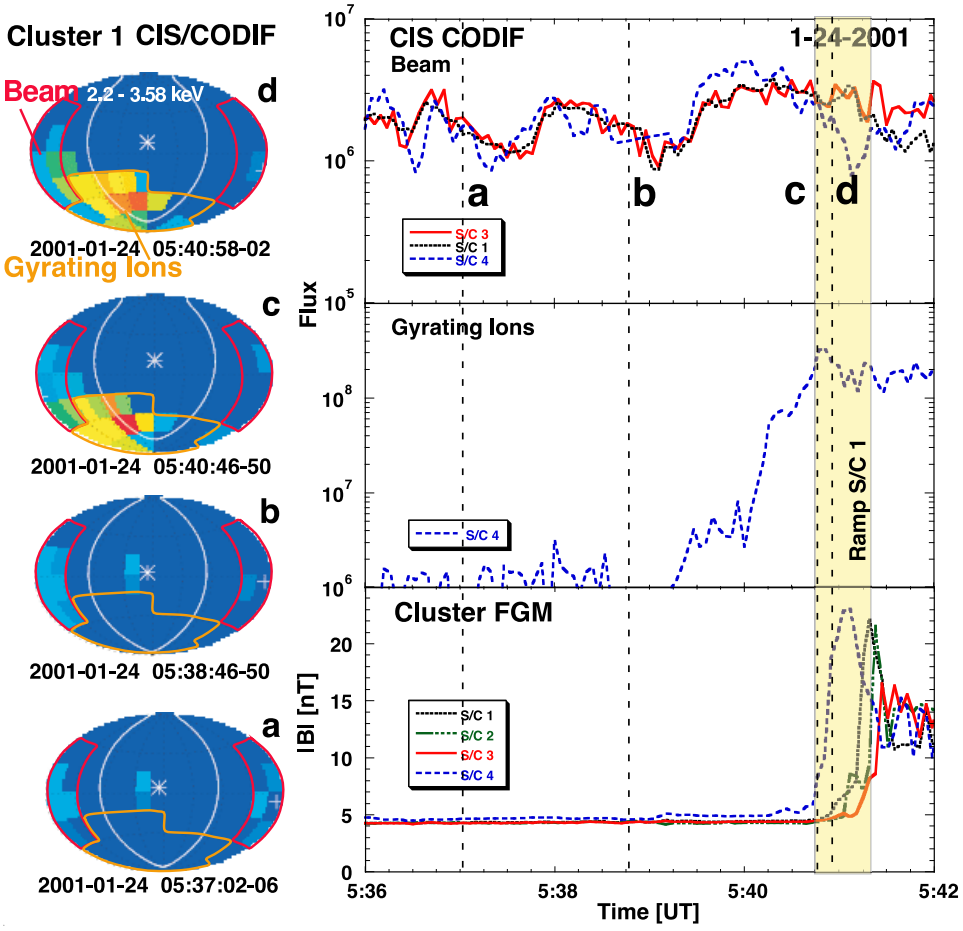

Figure 5.17. Left column: Angular distributions as seen on Cluster 1 in the shock ramp (d), at the ramp edge (c), and upstream of the shock (b, a). The angular regions of the beam (red) and ring (orange) are indicated; a '$+(*)$' denotes velocities in the direction $-(+)\mathbf{B}$. Right column: Integrated H^+ flux in the phase space portions that represent the beam from Cluster 1, 3 and 4 (upper panel), reflected ring from Cluster 4 (centre panel), and magnetic field strength from all four spacecraft (lower panel). They are shown from approximately 5 minutes before the bow shock encounter through the shock ramp. From Möbius et al. (2001).

From downstream of the shock through the shock ramp, the flux of the gyrating ion distribution (centre right panel in Fig. 5.17) remains high and falls off quickly by more than two orders of magnitude with distance from the shock. The remaining fluxes seen further upstream are on the level of one or a few counts and thus at the detection threshold for Cluster 4.

The total flux in the beam distribution is about one order of magnitude lower than that in the gyrating ions in the shock ramp, but it remains approximately constant (with quasi-regular fluctuations by a factor of three) with distance from the shock. The beam appears to originate in the combined reflected ion distribution in the shock ramp. It emerges from the edge of this wide pitch-angle distribution and then escapes more or less along the field lines under flux conservation. Therefore, the flux in the beam must depend on the angular width of the reflected distribution and on the original pitch-angle after ideal specular reflection in the shock potential. When relating the efficiency for beam generation to the shock parameters in comparison with models, these factors have to be taken into account in addition to the overall reflection efficiency for solar wind ions.

The results demonstrate quite clearly the value of two substantially different geometric factors in CODIF and of multi-spacecraft observations. While the high sensitivity side of CODIF is saturated by the ring distribution, which represents a large fraction of the solar wind flux, the low sensitivity side of CODIF is starved for counts in the beam distribution for the one-spin resolution observations used here. Only the split geometric factor allows for a simultaneous quantitative study of both, beam and gyrating ions. Furthermore, the high sensitivity side of CODIF, with a much higher count rate, shows remarkable structure and time variation in the beam. The beam flux varies substantially on a minute time scale, simultaneously on all spacecraft, while their distance from the shock differs, as indicated by the consecutive crossing of the shock: a clear indication for an intrinsic time variation of the beam. In addition, in view (a), i.e. substantially further upstream of the shock, the field aligned beam is more gyrotropic than about two minutes later. Closer to the shock the beam distribution apparently still has a memory of the original gyro-phase, with which it was injected at the shock. With increasing distance this memory effect is reduced because ions with different parallel velocities mix in gyrophase.

5.3.2 Source and generation of field-aligned beams

While the specular reflection of the gyrating ring distribution has been explained in a straight-forward manner as a reflection in the shock potential (Paschmann et al., 1980), the generation of the beam was not so readily understood. Although the kinematics and energetics of the beams can be derived correctly in terms of a perfect reflection of the incoming ions under energy conservation along the upstream IMF in the de Hofmann-Teller (dHT) frame (Sonnerup, 1969; Paschmann et al., 1980), the microphysics of their generation at the shock is still under debate. Con-

siderable progress has been made through the use of numerical simulations, commencing with hybrid simulations by Leroy and Winske (1983) and Burgess (1987) which explored the acceleration at the shock front itself. Field-aligned beam generation and so-called shock drift acceleration invoked at interplanetary and astrophysical shocks are, in fact, closely related phenomena (Burgess, 1987).

How can these ions escape upstream? The escape of the particles depends on their guiding centre motion, which has to carry them away from the shock along the field line against the convection of the magnetic field with the solar wind bulk flow. The escape speed increases enormously if θ_{Bn} approaches 90^o. Any process that can provide ions with high enough velocity parallel to the magnetic field so that their guiding centre velocity along the shock normal is larger than the convection speed will create an upstream ion beam. In principle beam ions can originate from downstream or from the shock ramp. However, as we shall see below, the physical processes responsible for the beam are still unknown. Additionally, although the case study of the preceding section suggests that the beam was drawn directly from the specularly reflected component, this has not yet been universally established.

5.3.2.1 Direct reflection under conservation of μ

A number of models to produce field-aligned ion beams have been proposed. Following the suggestion by Schwartz et al. (1983) we will discuss them within a similar representation in velocity space in the dHT-frame. This frame of reference simplifies the discussion as the flow of incoming ions is field-aligned and the motional electric field is zero. Figure 5.18 shows two possible scenarios of direct ion reflection at the bow shock. Sonnerup (1969) demonstrated that solar wind protons could easily be energised to form a rather energetic ion beam if the bow shock managed to turn the incoming ions around in such a way that they left the shock reasonably well field-aligned after reflection (left panel in Figure 5.18). He assumed that the particle energy was preserved in the dHT frame and the motion remained field-aligned after reflection, but he did not specify a reflection process. In observations with ISEE, Paschmann et al. (1980) actually found that the peak energy of ion beams as a function of the magnetic field orientation relative to the solar wind and to the shock normal agreed well with the prediction of this model.

This scenario is also referred to as 'adiabatic reflection' because of the apparent conservation of the magnetic moment μ. However, in observational studies (Paschmann et al., 1982) and numerical simulations (Leroy et al., 1981, 1982), μ is far from constant during ion reflection at the quasi-perpendicular bow shock. In their observations Paschmann et al. (1982) studied ions that were clearly specularly reflected by the shock potential. Such ions start to gyrate and then are swept downstream with the IMF, but do not show a field-aligned beam. This situation is shown in the right hand panel of Figure 5.18. The energy is conserved in the dHT frame in both scenarios, as indicated by the vectors for the reflected ion velocity ending on the same circle around the origin of the dHT frame. As a physical ion reflection

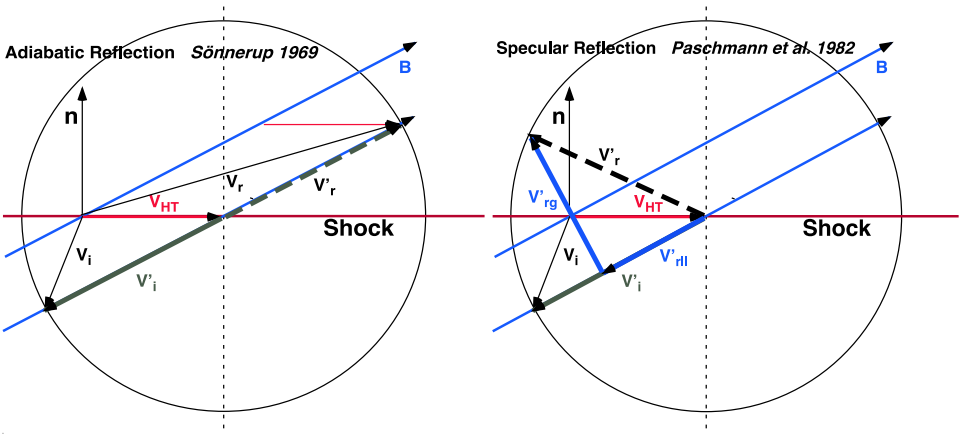

Figure 5.18. Kinematics of reflected ion beams and specularly reflected ions in velocity space at the quasi-perpendicular shock, shown in the de-Hoffmann-Teller (dHT) frame, i.e. translated along the shock with the dHT velocity V_{HT} so that there is no motional electric field. In this frame the incoming ions (V_i) arrive parallel to **B** (shown for upstream conditions) with V_i'. Ions that conserve energy in the dHT frame fall along the circle in velocity space. Left: Reflection along **B** under conservation of magnetic moment μ leads to escape along **B** with V_r' in the dHT frame and with V_r in the observer's frame (Sonnerup, 1969). Right: Specular reflection at the shock transforms part of the velocity into gyromotion (V_{rg}' perpendicular to **B**), and the velocity component parallel to **B**, $V_{r||}'$, of the reflected ion may point downstream or upstream, depending on θ_{Bn}. Figure adapted from Thomsen et al. (1983b) and other sources by E. Möbius.

mechanism that would conserve μ, Terasawa (1979) suggested the magnetic mirror force, but it cannot reflect solar wind ions at the shock because of their usually narrow pitch angle distribution. Apparently none of the known physical reflection mechanisms would cooperate toward the favourable energy condition found by Sonnerup (1969). Therefore, alternative generation mechanisms for beams were explored.

5.3.2.2 Leakage of heated magnetosheath ions

An alternate source for field-aligned beams could be leakage of magnetosheath ions that have been heated downstream of the shock. In an idealised model Edmiston et al. (1982) proposed that plasma is heated and thermalised in a thin layer at the shock front.

They calculated how ions from a hot Maxwellian distribution in this layer can return upstream. Magnetosheath ions, which arrive with zero velocity at the maximum of the shock potential, taken in the dHT frame, could be accelerated by falling through the potential drop at the shock ramp and escape parallel to **B**. However, in this model ions can only outrun the shock parallel to **B** and escape upstream for θ_{Bn} between 40^o and 55^o, yielding fractional densities up to at most 1%. For large θ_{Bn}

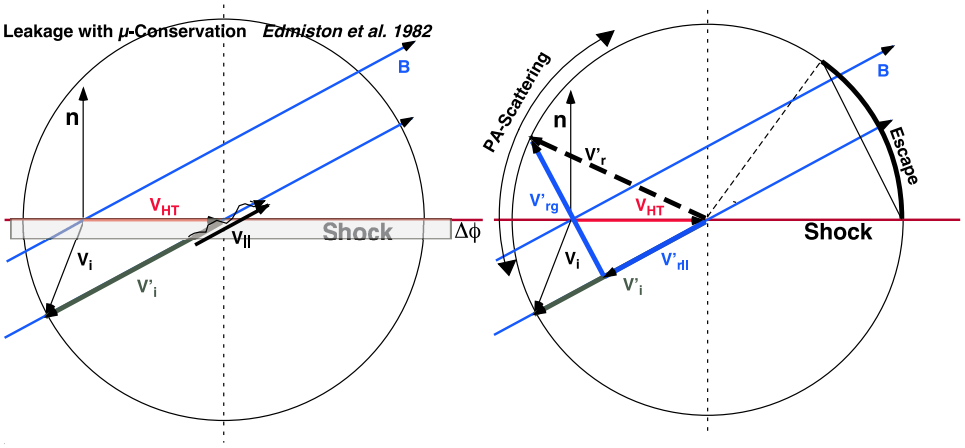

Figure 5.19. Kinematics of leakage and specularly reflected ions with subsequent pitch angle scattering in a similar representation as in Figure 5.18. Left: Leakage along **B** under conservation of magnetic momentum μ facilitated by the cross-shock potential $\Delta\phi$ (after Edmiston et al., 1982). Right: Specular reflection of incoming ions at the shock (after Paschmann et al., 1982) and subsequent pitch angle scattering with energy conservation in the dHT frame. Ions that get a large parallel velocity component away from the shock (dark section on the circle) can escape and form a beam-like distribution. Figure adapted from Thomsen et al. (1983b) and other sources by E. Möbius.

the parallel speed of the heated ions in the dHT frame is by far too small to allow escape. Because only the most energetic tail of the heated distribution downstream of the shock will even reach the top of the potential well at the shock with a speed ≥ 0, the peak of the emerging ion beam stems from those ions, which arrive with $v = 0$ and are ejected with a final speed equivalent to the shock potential (Schwartz et al., 1983). Ion distributions that are consistent with this picture, i.e. low energy ion beams at shocks with moderate values for θ_{Bn}, have been observed by Thomsen et al. (1983a).

Realising that the thickness of the layer with the shock potential is small compared with the ion gyro radii and that the ions most likely will not be magnetised during their transition of the shock, Schwartz et al. (1983) proposed a modified version of this model. They suggested that magnetosheath particles are accelerated by the shock potential mainly along the shock normal and that its component parallel to the magnetic field constitutes the resulting guiding centre motion back upstream. This poses an even more stringent constraint on the angles between shock normal and **B**, for which ions can escape upstream along the magnetic field, than the model by Edmiston et al. (1982).

Contrary to the earlier very local leakage scenarios, Tanaka et al. (1983) proposed a more self-consistent non-local model based on observations by Paschmann et al. (1982), simulations by Leroy et al. (1981), and the work by Edmiston et al. (1982). As solar wind encounters the quasi-perpendicular section of the bow shock,

part of the incoming solar wind distribution is specularly reflected and creates a gyrating ion distribution that is swept downstream. Its significant temperature anisotropy, due mainly to its high perpendicular temperature, is the source of free energy for electromagnetic ion cyclotron (EMIC) waves downstream of the shock. As a result, efficient pitch angle scattering will produce particles with a high enough velocity parallel to the magnetic field so that they can escape upstream, although test particle calculations suggest that ions have difficulty trying to leak from the magnetosheath (Burgess and Luhmann, 1986). Tanaka et al. (1983) pointed out that this model is consistent with a large fraction of the beams observed by Paschmann et al. (1980), but fails to explain the most energetic ion beams. This could indicate that direct reflection may also contribute to the production of ion beams.

In Figure 5.20 ISEE-2 observations of ion beams are compiled in comparison with the expectations according to the theoretical considerations mentioned above (Schwartz and Burgess, 1984). Shown is the bulk velocity of the beams normalised to the solar wind velocity parallel to the magnetic field in the dHT frame as a function of the shock normal angle θ_{Bn}. As already mentioned above part of the field aligned beams observed in the Earth's foreshock region with ISEE-2 appear to be consistent with the leakage hypothesis, while another fraction appears to support the relation found for adiabatic reflection. Almost all of them fall into the space between these relations as boundaries. However, it should be noted that the majority of the beams achieve velocities much higher than supported by leakage from downstream and that the adiabatic reflection hypothesis does not contain a physical reflection mechanism.

The recent observation with Cluster that the beam distribution and the specularly reflected ions are intimately connected and that the beam appears to emerge from the wing of the combined distribution (Möbius et al., 2001) provides important evidence of the processes responsible for the beam. Early work (Burgess and Schwartz, 1984) showed how pure dc fields at the shock could lead to some reflected ions suffering multiple encounters with the shock, as confirmed in later self-consistent simulations (Leroy and Winske, 1983; Burgess, 1987). Such particles, when viewed in the dHT frame, must emerge on the constant energy circle in Figure 5.19, and will escape upstream if after a final encounter they have sufficient parallel guiding centre velocity to prevent their return to the shock surface. Certainly, particles finding themselves in the fat dark portion of this circle marked 'escape' have persistently positive normal velocity and will escape. As the figure reveals, such particles have nearly the maximal beam speed as found from adiabatic reflection (Sonnerup, 1969), though the physics is quite different. In reality, a larger portion of the circle will result in escaping particles, and it is uncertain what the centroid of the total population would be, although simulations (Burgess, 1989) provide some indication. Whether it is best to describe this scenario as pitch angle diffusion/scattering is debatable. Scattering due to fluctuations and irregularities in the shock fields (e.g., within the foot, ramp, and/or overshoot regions) almost

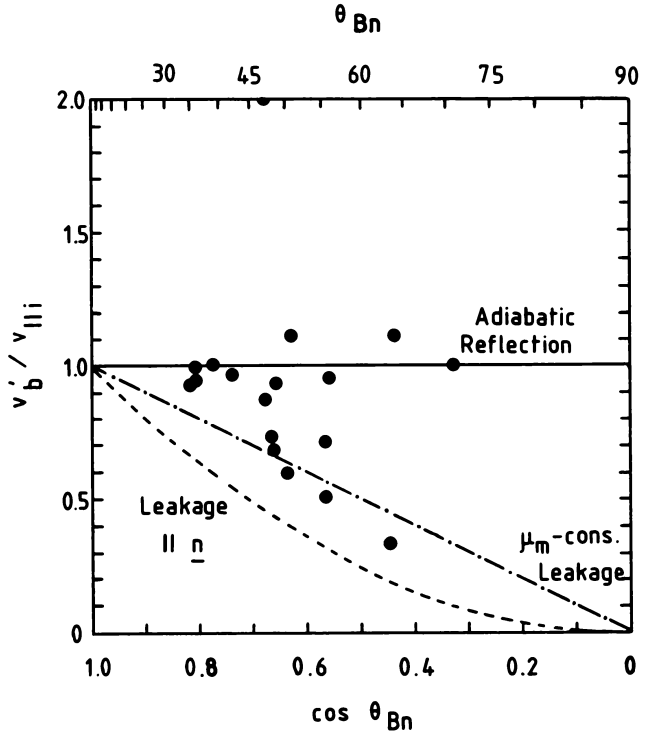

Figure 5.20. Observed velocity of ion beams normalised to the parallel component of the solar wind speed in the dHT frame as a function of the $\cos\theta_{Bn}$. The three curves represent the expected values for the three different ion beam generation models: Adiabatic reflection (Sonnerup, 1969), leakage under conservation of μ (Edmiston et al., 1982), and leakage with acceleration parallel to the shock normal. From Schwartz et al. (1983).

certainly does not preserve kinetic energy in the dHT frame, as such fluctuations propagate at relatively small speeds relative to the bulk plasma flow. Nonetheless, they may play a role, as yet unquantified, in aiding (or hindering) the dc process of multiple shock encounters, or in masking those effects and otherwise diffusing the distribution in velocity space.

A note of caution may be in order. The simple dependence on the local shock normal angle is a direct consequence of the assumption of a planar, featureless, and stationary bow shock. In a way, the predicted and often observed energy dependence on θ_{Bn} may just reflect the necessary escape condition for ion beams. In this picture, it is assumed implicitly that the dHT frame is natural frame of reference, which implies that the reflection and scattering happens in this frame and for a comparison with observations that all parameters for the transformation are known and reasonably constant over the integration period. Any motion of the

shock and/or local structures that deviate from a planar shock with the assumed normal may complicate a quantitative comparison with a specific model or even with the simple escape condition.

5.3.2.3 Cluster observations on leakage vs. reflection

The initial results from Cluster have demonstrated that the field-aligned ion beams emerge from the reflected gyrating ion distributions. More recent Cluster studies by Kucharek et al. (2004) suggest a resolution on the source region for the beams. They analysed several quasi-perpendicular shock crossings with CIS and followed the spatial and temporal evolution of the reflected and transmitted ion populations across the shock. Figure 5.21 shows a composite plot during the crossing at 18:48 UT on March 31, 2001, from downstream to upstream, including a snapshot in the shock ramp. The upper panel shows the magnetic field as a function of time, and in the lower panel the ion distributions, parallel and perpendicular to the interplanetary magnetic field (the mean magnetic field orientation is indicated by arrows), are shown for three different locations: downstream, at the ramp, and upstream of the bow shock. The dark blue shaded areas in the magnetic field profile indicate the integration times for the ion distributions. Downstream, the shape of the ion distribution is more elongated perpendicular to the magnetic field. The phase space is filled with ions up to a parallel velocity of $1000\,\mathrm{km\,s^{-1}}$. In the shock ramp, gyrating ions appear whose phase space density extends in parallel velocity, exceeding substantially the limit of $v \approx 1000\,\mathrm{km\,s^{-1}}$. Upstream of the shock (right hand distribution), this part of the distribution decouples from the core and forms a collimated beam along the mean interplanetary magnetic field. It should be noted that the beam occupies a portion of the phase space that is empty downstream.

Such simultaneous observations at different locations at the vicinity of the quasi-perpendicular bow shock indicate that the field-aligned beams most likely result from effective scattering in pitch-angle during reflection in the shock ramp. At least in this low Mach number shock, leakage of thermalized ions from the downstream region does not appear to be the source. While Figure 5.21 presents consecutive observations with Cluster 1, Kucharek et al. (2004) also studied a shock crossing for which simultaneous observations in the shock ramp and upstream are available (their Fig. 6, not shown here). The same pattern as described here is observed in this case.

From their results Kucharek et al. (2004) concluded that processes right in the shock ramp must produce the ion beams. Therefore, scattering in the shock ramp seems to be a major process that is responsible for their generation, which appears to be in accordance with findings from simulations by Scholer et al. (2000).

In their study Kucharek et al. (2004) also find a low intensity field-aligned ion beam upstream of a low Mach number supercritical shock at a rather large shock normal angle ($\theta_{Bn} = 74.5^o$). Interestingly enough it appears as if the basic escape condition might be violated and the conditions are far from reflection under con-

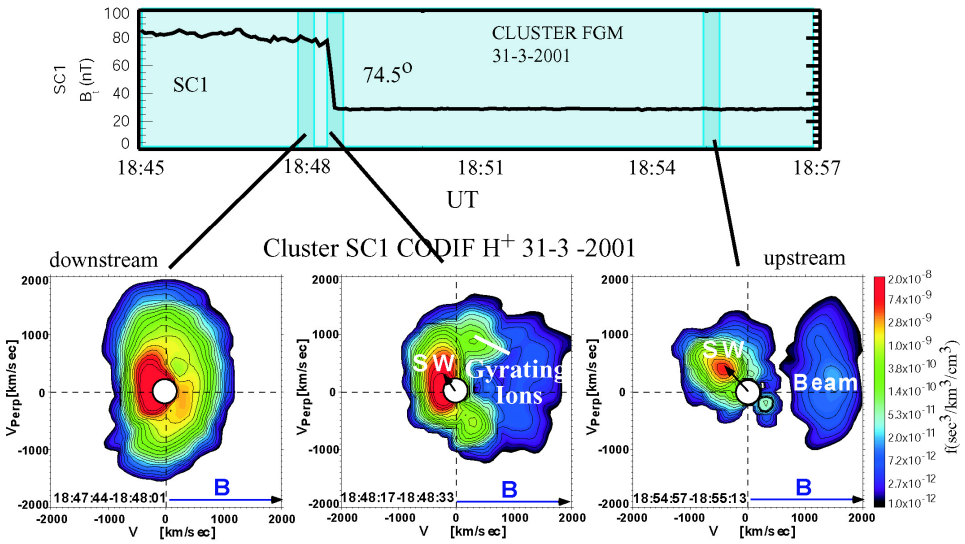

Figure 5.21. Magnetic field (top panel) and ion velocity space distributions (lower panel) downstream, in the ramp, and upstream of a quasi-perpendicular shock. Note that the upstream beam occupies portions of velocity space which are empty downstream, implying that the beams emerge directly from processes within the shock layer. From Kucharek et al. (2004).

servation of the magnetic moment. They point out that the dynamic structure of the bow shock at these large shock normal angles may be important for the visibility of field-aligned beams.

It is commonly known that the Earth's bow shock is a dynamic structure, which responds both locally and globally to changes of the solar wind conditions. During the crossing shown in Figure 5.21 that is associated with the ion beam the bow shock is receding with a velocity of about 30 km s^{-1}toward the Earth. During the preceding crossing, which is not associated with an ion beam (not shown here), the shock is approaching the spacecraft. Both motions result in much larger velocities along the magnetic field, thus necessitating a re-evaluation of the escape condition in a frame that is corrected for the shock motion. With such a correction the escape conditions for the ions are most probably marginally fulfilled for the crossing at 18:47 UT, whereas at 18:30 UT they are not. In none of the models has the dynamic structure of the Earth's bow shock in response to changes of the solar wind been taken into account thus far. The multi-spacecraft capabilities of Cluster provide the tools to include them in the models and to test them with actual observations.

5.3.3 Composition of field-aligned ion beams

Thus far mainly protons in field-aligned beams have been investigated. Compositional studies have been performed by Fuselier and Thomsen (1992) and Ipavich

et al. (1988). These studies show that field-aligned ion beams consist almost entirely of protons and contain very little helium. In their survey (with 14 –23 field-aligned ion beams) these authors find that the proton beams reach a density of $< 1\%$ of the solar wind density. The most surprising finding however is the extremely low He^{2+}/H^{+} beam density ratio of $\sim 5 \times 10^{-4}$. This value is about two orders of magnitude lower than the nominal solar wind ratio. This low He^{2+} abundance has implications on the source and generation of field-aligned beams. It appears to be compatible with the finding by Möbius et al. (2001) that beams emerge from the gyrating ion distribution. While solar wind protons are specularly reflected by the shock potential with good efficiency, this seems not to be the case for solar wind He^{2+} (Fuselier and Schmidt, 1994). As a consequence they should be suppressed in their abundance in field-aligned beams as well. For beam events that arise from leakage, higher abundances may be found. It will therefore be an important task in further studies with Cluster to determine He^{2+} abundance values for field-aligned beams and specularly reflected ions.

5.3.4 Discussion on the nature of field-aligned beams

In the past reflected gyrating ions and ion beams at quasi-perpendicular shocks were discussed as two separate and different populations. Recent observations with Cluster have shown that the distribution of the beam ions originates from gyrating ions in the shock ramp. Cluster multi-spacecraft observations support the following, more generalised formation mechanism of field-aligned beams at the quasi-perpendicular Earth's bow shock: Part of the incoming solar wind is reflected and accelerated at the shock to form a gyrating ion distribution. Pitch angle scattering in the shock ramp will produce a small fraction of the gyrating ions which have a high velocity parallel to the magnetic field. Those ions from this scattered distribution that have a velocity component parallel to the shock normal larger than the convection speed of interplanetary magnetic field at the shock ramp will escape upstream and form a field-aligned ion beam. The intensity of the ion beam upstream will then be determined by pitch angle scattering in the shock ramp and not only by the shock geometry. Fluxes of ion beams show significant differences between the spacecraft and vary with time, which seems to reflect spatial and temporal variations.

Surprisingly, Cluster also observed field-aligned ion beams at very high shock normal angles. It appeared as if for this event (see Figure 5.21) the escape condition is violated and that the beam energy is far from that obtained by assuming reflection in the dHT frame under conservation of energy. At this high shock normal angle the beam ions should not be able to escape upstream. However, perpendicular shocks are dynamic and small-scale structures can lead to a deviation of the average θ_{Bn}. Both can modify the critical conditions so that ions can escape upstream. Therefore, it has been pointed out that processes right in the shock ramp

and the dynamics of the shock itself seems to be the major production mechanism of these ion beams.

Although Cluster has already provided interesting new insight into processes and sources of ion beams upstream of the Earth's bow shock, many questions are still unanswered. Cluster will contine to contribute to the resolution of these problems with its unique capabilities. For instance: what determines the fraction of reflected ions that forms the gyration ion distribution? What fraction of these ions will escape upstream? What are the critical shock parameters that control the ion beam formation? How important is the internal structure of the shock, and what is the impact of the shock potential on particle reflection and acceleration?

5.4 Summary

The Earth's bow shock represents the most studied example of a collisionless shock. The bow shock under quasi-perpendicular conditions, where the magnetic field is nearly perpendicular to the shock normal, is the most exhaustively scrutinised form due primarily to its relatively clean, characteristic shape and features. Despite a considerable body of pre-existing knowledge, Cluster has contributed several important new results. These results take full advantage of Cluster's unique 4-spacecraft ability to disentangle space and time, and so to infer shape, orientation, static vs. dynamic processes, and simultaneous 3D measurements. These results include:

1. Confirmation that the overall shape of the bow shock, and its motion, are well-represented by previous statistical investigations.

2. Proof that the density and magnetic field ramp widths are governed by a trapped ion gyroscale rather than an ion inertial length. This places severe constraints on the dispersive and dissipative processes which effect the overall shock transition.

3. Identification of small scale electric field spikes within the overall shock transition which appear to be universally present. Their role in the overall shock dynamics remains to be elucidated.

4. Demonstration that much of the variability in the shock profile is confined to the magnetic foot, rather than main ramp, regions. This implies that although ion reflection and dynamics are responsible for the foot appearance, and also for the overall transition scale (as noted above), the main shock ramp and dissipation are not dependent on the fine details of the ion reflection process.

5. Demonstration that energetic field aligned beams of ions observed backstreaming from the bow shock are generated and accelerated at the shock following an initial reflection process.

Other related Cluster results, such as the interaction of field-aligned beams with the upstream wave-field, and the back-reaction of the wave field on the local shock processes, can be found in Eastwood et al. (2005, this issue).

All these results reveal the power of Cluster's multi-spacecraft strategy, and leave open a rich dataset capable of addressing many more outstanding questions on the subject of collisionless shocks under quasi-perpendicular conditions.

Acknowledgements

The contributions of HK and EM were partially supported under NASA Grants NAG5-10131 and NAG5-11804. PPARC (UK) support for this work includes fellowships (TSH and EL) and research grants (DB, SJS, SNW).

References

Asbridge, J. R., S. J. Bame, and I. B. Strong: 1968, 'Outward flow of protons from the Earth's bow shock'. *J. Geophys. Res.* **73**(12), 5777.

Bagenal, F., J. W. Belcher, E. C. Sittler, Jr., and R. P. Lepping: 1987, 'The Uranian Bow Shock: Voyager 2 Inbound Observations of a High Mach Number Shock'. *J. Geophys. Res.* **92**, 8603.

Bale, S. D., F. S. Mozer, and T. S. Horbury: 2003, 'Density-transition scale at quasiperpendicular collisionless shocks'. *Physical Review Letters* **91**(26), 265004.

Balikhin, M., M. Gedalin, and A. Petrukovich: 1995, 'The scales in quasiperpendicular shocks'. *Adv. Space. Res.* **15**, 247.

Balikhin, M., V. Krasnosel'skikh, and M. Gedalin: 1993, 'New mechanism for heating in shocks'. *Phys. Rev. Lett.* **70**, 1259.

Balikhin, M. A., M. Nozdrachev, M. Dunlop, V. Krasnosel'skikh, S. N. Walker, H. S. K. Alleyne, V. Formisano, M. André, A. Balogh, A. Eriksson, and K. Yearby: 2002, 'Observation of the terrestrial bow shock in quasi-electrostatic sub-shock regime'. *J. Geophys. Res.* **107**, 1155, doi: 1029/2001JA000327.

Bame, S. J., J. R. Asbridge, W. C. Feldman, J. T. Gosling, G. Paschmann, and N. Sckopke: 1980, 'Deceleration of the solar wind upstream from the Earth's bow shock and the origin of diffuse upstream ions'. *J. Geophys. Res.* **85**(14), 2981–2990.

Bonifazi, C. and G. Moreno: 1981, 'Reflected and diffuse ions backstreaming from the earth's bow shock. I Basic properties'. *J. Geophys. Res.* **86**(15), 4397–4413.

Burgess, D.: 1987, 'Shock drift acceleration at low energies'. *J. Geophys. Res.* **92**(11), 1119–1130.

Burgess, D.: 1987, 'Simulations of backstreaming ion beams formed at oblique shocks by direct reflection'. *Ann. Geophys.* **5**, 133–145.

Burgess, D.: 1989, 'Alpha particles in field-aligned beams upstream of the bow shock - Simulations'. *Geophys. Res. Lett.* **16**, 163–166.

Burgess, D. and J. G. Luhmann: 1986, 'Scatter-free propagation of low energy protons in the magnetosheath: Implications for the production of field-aligned beams by non-thermal leakage'. *J. Geophys. Res.* **91**, 1439–1449.

Burgess, D. and S. J. Schwartz: 1984, 'The dynamics and upstream distributions of ions reflected at the Earth's bow shock'. *J. Geophys. Res.* **89**(18), 7407–7422.

Dunlop, M. W., A. Balogh, and K.-H. Glassmeier: 2002, 'Four-point Cluster application of magnetic field analysis tools: The discontinuity analyzer'. *J. Geophys. Res.* **107**, 1385, doi:10.1029/2001JA005089.

Dunlop, M. W. and T. I. Woodward: 1998, 'Discontinuity analysis: Orientation and motion'. In: *Analysis Methods for Multispacecraft Data*, Vol. ISSI Sci. Rep. SR-001. Norwell, Mass.: Kluwer Acad., p. 271.

Eastwood, J., E. A. Lucek, C. Mazelle, K. Meziane, Y. Narita, J. Pickett, and R. Treumann: 2005, 'The Foreshock'. *Space Sci. Rev.* **this issue**.

Edmiston, J., C. Kennel, and D. Eichler: 1982, 'Escape of heated ions upstream of quasi-parallel shocks'. *Geophys. Res. Lett.* **9**, 531–534.

Eselevich, V. G.: 1982, 'Shock-wave structure in collisionless plasmas from results of laboratory experiments'. *Space Science Reviews* **32**, 65–81.

Eselevich, V. G., A. G. Eskov, R. C. Kurtmullaev, and A. I. Malyutin: 1971, 'Isomagnetic discontinuity in a collisionless shock wave'. *Soviet Phys. JETP* **33**, 1120.

Farris, M. H. and C. T. Russell: 1994, 'Determining the standoff distance of the bow shock: Mach number dependence and use of models'. *J. Geophys. Res.* **99**(18), 17681.

Formisano, V.: 1979, 'The three-dimensional shape of the bow shock'. *Nuovo Cimento C Geophysics Space Physics C* **2**, 681–692.

Formisano, V.: 1982, 'Measurement of the potential drop across the Earth's collisionless bow shock'. *Geophys. Res. Lett.* **9**, 1033.

Formisano, V.: 1985, 'Collisionless shock waves in space and astrophysical plasmas'. In: *Proc. ESA workshop on future missions in solar, heliospheric and space plasma physics*, Vol. ESA SP-235. p. 83.

Formisano, V. and R. Torbert: 1982, 'Ion acoustic wave forms generated by ion-ion streams at the Earth's bow shock'. *Geophys. Res. Lett.* **9**, 207.

Fuselier, S. and M. F. Thomsen: 1992, 'He^{2+} in field-aligned beams: ISEE results'. *Geophys. Res. Lett.* **19**, 437.

Fuselier, S. A. and W. K. H. Schmidt: 1994, 'H^+ and He^{2+} heating at the Earth's bow shock'. *J. Geophys. Res.* **99**(18), 11539–11546.

Galeev, A. A., C. F. Kennel, V. V. Krasnoselskikh, and V. V. Lobzin: 1988a, 'Quasiperpendicular collisionless high Mach number shocks'. In: *Proc. Joint Varenna-Abastumani Int. School & Workshop on Plasma Astrophysics, Varenna, Italy, 24 Aug - 3 September*. pp. 173–183.

Galeev, A. A., C. F. Kennel, V. V. Krasnoselskikh, and V. V. Lobzin: 1988b, 'The role of whistler oscillations in the formation of the structure of high Mach number collisionless shock'. In: *Proc. Joint Varenna-Abastumani Int. School & Workshop on Plasma Astrophysics, Varenna, Italy, 24 Aug - 3 September*. pp. 165–171.

Galeev, A. A., V. V. Krasnoselskikh, and V. V. Lobzin: 1988c, 'On the fine structure of the quasiperpendicular supercritical collisonless shock,'. *Sov. J. Plasma Phys.* **14**, 697.

Gedalin, M. and E. Griv: 1999, 'Role of overshoots in the formation of the downstream distribution of adiabatic electrons'. *J. Geophys. Res.* **104**(13), 14821–14826.

Giacalone, J., T. P. Armstrong, and R. B. Decker: 1991, 'Effect of magnetic overshoot on shock drift acceleration'. *J. Geophys. Res.* **96**(15), 3621–3626.

Gosling, J. T., J. R. Asbridge, S. J. Bame, G. Paschmann, and N. Sckopke: 1978, 'Observations of two distinct populations of bow shock ions in the upstream solar wind'. *Geophys. Res. Lett.* **5**, 957–960.

Gosling, J. T. and A. E. Robson: 1985, 'Ion reflection, gyration, and dissipation at supercritical shocks'. In: B. Tsurutani and R. Stone (eds.): *Collisionless Shocks in the Heliosphere: Reviews of current research*, Geophys. Monogr. Ser. vol 35. Washington, D.C.: American Geophysical Union, pp. 141–152.

Greenstadt, E. W., C. T. Russell, and M. Hoppe: 1980, 'Magnetic field orientation and suprathermal ion streams in the Earth's foreshock'. *J. Geophys. Res.* **85**(.14), 3473–3479.

Gustafsson, G., R. Boström, B. Holback, G. Holmgren, A. Lundgren, K. Stasiewicz, L. Åéhlen, F. S. Mozer, D. Pankow, P. Harvey, P. Berg, R. Ulrich, A. Pedersen, R. Schmidt, A. Butler, A. W. C. Fransen, D. Klinge, M. Thomsen, C.-G. Falthammar, P.-A. Lindqvist, S. Christenson, J. Holtet, B. Lybekk, T. A. Sten, P. Tanskanen, K. Lappalainen, and J. Wygant: 1997, 'The electric field and wave experiment for the Cluster mission'. *Space Sci. Rev.* **79**, 137–156.

Hada, T., M. Oonishi, B. Lembège, and P. Savoini: 2003, 'Shock front nonstationarity of supercritical perpendicular shocks'. *J. Geophys. Res.* **108**, 1233, doi:10.1029/2002JA009339.

Hellinger, P., P. Trávnícek, and H. Matsumoto: 2002, 'Reformation of perpendicular shocks: Hybrid simulations'. *Geophys. Res. Lett.* **29**, 2234, doi:10.1029/2002GL015915.

Heppner, J. P., N. C. Maynard, and T. L. Aggson: 1978, 'Early results from ISEE-1 electric field measurements'. *Space Sci. Rev.* **22**, 777.

Heppner, J. P., M. Sugiura, T. L. Skillman, B. G. Ledley, and M. Campbell: 1967, 'OGO-A magnetic field observations'. *J. Geophys. Res.* **72**(11), 5417.

Horbury, T. S., P. Cargill, E. A. Lucek, A. Balogh, M. W. Dunlop, T. Oddy, C. Carr, A. Szabo, and K.-H. Fornacon: 2001, 'Cluster magnetic field observations of the bowshock: Orientation, motion and structure'. *Ann. Geophys.* **19**, 1399–1409.

Horbury, T. S., P. J. Cargill, E. A. Lucek, J. Eastwood, A. Balogh, M. W. Dunlop, K.-H. Fornaçon, and E. Georgescu: 2002, 'Four spacecraft measurements of the quasi-perpendicular terrestrial bowshock: Orientation and motion'. *J. Geophys. Res.* **107**(A8), 1208, doi 10.1029/2001JA000273.

Ipavich, F. M., G. Gloeckler, D. Hamliton, and L. Kistler: 1988, 'Protons and alpha particles in field-aligned beams upstream of the bow shock'. *Geophys. Res. Lett.* **15**, 1153.

Karpman, V. I.: 1964, 'Structure of the shock front propagating at an angle of the magnetic field in a low density plasma'. *Sov. Phys. Tech. Phys. Engl. Trans.* **8**, 715.

Kennel, C. F., J. P. Edmiston, and T. Hada: 1985, 'A quarter century of collisionless shock research'. *Washington DC American Geophysical Union Geophysical Monograph Series* **34**, 1–36.

Krasnosel'skikh, V. V.: 1985, 'Nonlinear plasma motions across the magnetic field'. *Sov. Phys. JETP* **62**, 282.

Krasnosel'skikh, V. V., T. Vinogradova, M. A. Balikhin, H. S. C. Alleyne, A. K. Pardaens, L. J. C. Woolliscroft, S. I. Klimov, A. Petrukovich, W. A. C. Mier-Jedrzejowicz, and D. J. Southwood: 1991, 'On the nature of low frequency turbulence in the foot of strong quasi-perpendicular shocks'. *Advances in Space Research* **11**, 15–18.

Krasnosselskikh, V., B. Lemb'ege, P. Savoini, and V. V. Lobzin: 2002, 'Nonstationarity of strong collisionless quasiperpendicular shocks: Theory versus full particle numerical simulations'. *Phys. Plasmas* **9**(4), 1192.

Kucharek, H., E. Möbius, M. Scholer, C. Mouikis, L. Kistler, T. Horbury, A. Balogh, H. Réme, and J. Bosqued: 2004, 'On the origin of field-aligned beams at the quasi-perpendicular bow shock: Multi-spacecraft observations by Cluster'. *Ann. Geophys.* **22**, 2301–2308.

Lembège, B. and J. M. Dawson: 1987a, 'Plasma heating through a supercritical oblique collisionless shock'. *Physics of Fluids* **30**, 1110–1114.

Lembège, B. and J. M. Dawson: 1987b, 'Self-consistent study of a perpendicular collisionless and nonresistive shock'. *Physics of Fluids* **30**, 1767–1788.

Lembège, B. and P. Savoini: 1992, 'Nonstationarity of a two-dimensional quasiperpendicular supercritical collisionless shock by self-reformation'. *Physics of Fluids B* **4**, 3533–3548.

Lembège, B., S. N. Walker, P. Savoini, M. A. Balikhin, and V. Krasnosel'skikh: 1999, 'The spatial sizes of electric and magnetic field gradients in a simulated shock'. *Adv. Space. Res.* **24**, 109–112.

Lepidi, S., U. Villante, and A. J. Lazarus: 1997, 'Single spacecraft identification of the bow shock orientation and speed: A comparison between different methods'. *Nuovo Cimento C Geophysics Space Physics C* **20**, 911.

Leroy, M. M., C. C. Goodrich, D. Winske, C. S. Wu, and K. Papadopoulos: 1981, 'Simulation of a perpendicular bow shock'. *Geophys. Res. Lett.* **8**, 1269–1272.

Leroy, M. M. and D. Winske: 1983, 'Backstreaming ions from oblique Earth bow shocks'. *Annales Geophysicae* **1**, 527–536.

Leroy, M. M., D. Winske, C. C. Goodrich, C. S. Wu, and K. Papadopoulos: 1982, 'The structure of perpendicular bow shocks'. *J. Geophys. Res.* **87**, 5081.

Liewer, P. C., V. K. Decyk, J. M. Dawson, and B. Lembège: 1991, 'Numerical studies of electron dynamics in oblique quasi-perpendicular collisionless shock waves'. *J. Geophys. Res.* **96**, 9455.

Lin, R. P., C. I. Meng, and K. A. Anderson: 1974, '30 -100 keV protons upstream from the Earth bow shock'. *J. Geophys. Res.* **79**, 489.

Livesey, W. A., C. F. Kennel, and C. T. Russell: 1982, 'ISEE-1 and -2 observations of magnetic field strength overshoots in quasi-perpendicular bow shocks'. *Geophys. Res. Lett.* **9**, 1037–1040.

Livesey, W. A., C. T. Russell, and C. F. Kennel: 1984, 'A comparison of specularly reflected gyrating ion orbits with observed shock foot thicknesses'. *J. Geophys. Res.* **89**(18), 6824–6828.

Maksimovic, M., S. D. Bale, T. S. Horbury, and M. André: 2003, 'Bow shock motions observed with CLUSTER'. *Geophys. Res. Lett.* **30**, 1393, doi:10.1029/2002GL016761.

Meziane, K., C. Mazelle, M. Wilber, D. Lequéau, J. Eastwood, H. Rème, I. Dandouras, J. Sauvaud, J. Bosqued, G. Parks, L. Kistler, M. McCarthy, B. Klecker, A. Korth, M. Bavassano-Cattaneo, R. Lundin, and A. Balogh: 2004, 'Bow shock specularly reflected ions in the presence of low-frequency electromagnetic waves: A case study'. *Annales Geophysicae* **22**, 2325–2335.

Möbius, E., H. Kucharek, C. Mouikis, E. Geogescu, L. M. Kistler, M. A. Popecki, M. Scholer, J. M. Bosqued, H. Réme, C. W. Carlson, B. Klecker, A. Korth, G. K. Parks, J. C. Sauvand, H. Balsiger, M.-B. Bavassano-Cattaneu, I. Dandouras, A. M. DiLellis, L. Eliasson, V. Formisano, T. Hobury, W. Lennartson, R. Lundin, M. McCarthy, J. McFadden, and G. Paschmann: 2001, 'Observation of the spatial and temporal structure of field-aligned beam and gyrating ring distributions at the quasi-perpendicular bow shock with Cluster CIS'. *Ann. Geophys.* **19**, 1411.

Morse, D. L.: 1976, 'A model for ion thermalization in the Earth's bow shock'. *J. Geophys. Res.* **81**(10), 6126–6130.

Morse, D. L., W. W. Destler, and P. L. Auer: 1972, 'Nonstationary behavior of collisionless shocks'. *Physical Review Letters* **28**, 13–16.

Newbury, J. A. and C. T. Russell: 1996, 'Observations of a very thin collisionless shock'. *Geophys. Res. Lett.* **23**, 781.

Papadopoulos, K.: 1985, 'Microinstabilities and anomalous transport'. *Washington DC American Geophysical Union Geophysical Monograph Series* **34**, 59–90.

Paschmann, G., N. Sckopke, I. Papamastorakis, J. R. Asbridge, S. J. Bame, and J. T. Gosling: 1981, 'Characteristics of reflected and diffuse ions upstream from the earth's bow shock'. *J. Geophys. Res.* **86**(15), 4355–4364.

Paschmann, G. and P. W. Daly (eds.): 1998, *Analysis methods for multi-spacecraft data*, ISSI Sci. Rep. SR-001. Bern: ISSI.

Paschmann, G., N. Sckopke, S. J. Bame, and J. Gosling: 1982, 'Observations of gyrating ions in the foot of the nearly perpendicular bow shock'. *Geophys. Res. Lett.* **9**, 881.

Paschmann, G., N. Sckopke, I. Papamastorakis, J. Asbridge, S. Bame, and J. Gosling: 1980, 'Energetization of solar wind ions by reflection from the Earth's bow shock'. *J. Geophys. Res.* **85**, 4689.

Peredo, M., J. A. Slavin, E. Mazur, and S. A. Curtis: 1995, 'Three-dimensional position and shape of the bow shock and their variation with Alfvenic, sonic and magnetosonic Mach numbers and interplanetary magnetic field orientation'. *J. Geophys. Res.* **100**(9), 7907–7916.

Quest, K. B.: 1985, 'Simulations of high-Mach-number collisionless perpendicular shocks in astrophysical plasmas'. *Physical Review Letters* **54**, 1872–1874.

Quest, K. B.: 1986, 'Simulations of high Mach number perpendicular shocks with resistive electrons'. *J. Geophys. Res.* **91**(10), 8805–8815.

Russell, C. T. and E. W. Greenstadt: 1979, 'Initial ISEE magnetometer results - Shock observation'. *Space Science Reviews* **23**, 3–37.

Saxena, R., S. D. Bale, and T. S. Horbury: 2004, 'Wavelength and decay length of density overshoot structure at supercritical, collisionless bow shocks'. *Phys. of Plasmas* p. submitted.

Scholer, M., H. Kucharek, and J. Giacalone: 2000, 'Cross-field diffusion of charged particles and the problem of ion injection and acceleration at quasi-perpendicular shocks'. *J. Geophys. Res.* **105**, 18285.

Scholer, M., I. Shinohara, and S. Matsukiyo: 2003, 'Quasi-perpendicular shocks: Length scale of the cross-shock potential, shock reformation, and implication for shock surfing'. *J. Geophys. Res.* **108**, 1014, doi:10.1029/2002JA009515.

Schwartz, S. J.: 1998, 'Shock and discontinuity normals, Mach numbers, and related parameters'. In: G. Paschmann and P. W. Daly (eds.): *Analysis methods for multi-spacecraft data*, ISSI Sci. Rep. SR-001. Bern: ISSI, pp. 249–270.

Schwartz, S. J. and D. Burgess: 1984, 'On the theoretical/observational comparison of field-aligned ion beams in the Earth's foreshock'. *J. Geophys. Res.* **89**, 2381 – 2384.

Schwartz, S. J., M. F. Thomsen, and J. Gosling: 1983, 'Ions upstream of the earth's bow shock: A theoretical comparison of alternative source populations'. *J. Geophys. Res.* **88**, 2039–2047.

Sckopke, N., G. Paschmann, S. J. Bame, J. T. Gosling, and C. T. Russell: 1983, 'Evolution of ion distributions across the nearly perpendicular bow shock - Specularly and non-specularly reflected-gyrating ions'. *J. Geophys. Res.* **88**(17), 6121–6136.

Sckopke, N., G. Paschmann, A. L. Brinca, C. W. Carlson, and H. Lühr: 1990, 'Ion thermalization in quasi-perpendicular shocks involving reflected ions'. *J. Geophys. Res.* **95**, 6337.

Scudder, J. D.: 1995, 'A Review of the Physics of Electron Heating at Collisionless shocks'. *Adv. Space. Res.* **15**, 181.

Scudder, J. D., T. L. Aggson, A. Mangeney, C. Lacombe, and C. C. Harvey: 1986, 'The resolved layer of a collisionless, high beta, supercritical, quasi-perpendicular shock wave. II - Dissipative fluid electrodynamics'. *J. Geophys. Res.* **91**(10), 11053–11073.

Sibeck, D. G., R. E. Lopez, and E. C. Roelof: 1991, 'Solar wind control of the magnetopause shape, location, and motion'. *J. Geophys. Res.* **96**(15), 5489–5495.

Sonnerup, B. U. O.: 1969, 'Acceleration of particles reflected at a shock front'. *J. Geophys. Res.* **74**, 1301.

Spreiter, J. R., A. L. Summers, and A. Y. Alksne: 1966, 'Hydromagnetic flow around the magnetosphere'. *Planet. Space Sci.* **14**, 223–223.

Tanaka, M., C. C. Goodrich, D. Winske, and K. Papadopoulos: 1983, 'A Source of the backstreaming ion beams in the foreshock region'. *J. Geophys. Res.* **88**, 3046.

Terasawa, T.: 1979, 'Energy spectrum and pitch angle distribution of particles reflected by MHD shock waves of the fast mode'. *Planet. Space Sci.* **27**, 193.

Thomsen, M.: 1985, 'Upstream suprathermal ions'. In: B. Tsurutani and R. Stone (eds.): *Collisionless Shocks in the Heliosphere: Reviews of current research*, Geophys. Monogr. Ser. vol 35. Washington, D.C.: American Geophysical Union, pp. 253–270.

Thomsen, M. F., J. T. Gosling, S. J. Bame, W. C. Feldman, G. Paschmann, and N. Sckopke: 1983a, 'Field-aligned beams upstream of the Earth's bow shock: Evidence for a magnetosheath source'. *Geophys. Res. Lett.* **10**, 1207–1210.

Thomsen, M. F., S. J. Schwartz, and J. T. Gosling: 1983b, 'Observational evidence on the origin of ions upstream of the earth's bow shock'. *J. Geophys. Res.* **88**, 7843–7852.

Tsurutani, B. T. and R. G. Stone: 1985, 'Collisionless shocks in the heliosphere: Reviews of current research'. *Washington DC American Geophysical Union Geophysical Monograph Series* **35**.

Vaisberg, O., S. Klimov, G. Zastenker, M. Nozdrachev, A. Sokolov, V. Smirnov, S. Savin, and L. Avanov: 1984, 'Relaxation of plasma at the shock front'. *Adv. Space. Res.* **4**, 265–275.

Vaisberg, O., G. Zastenker, V. Smirnov, Z. Nemecek, and J. Safrankova: 1986a, 'Ion distribution function dynamics near the strong shock front (Project Intershock)'. *Advances in Space Research* **6**, 41–44.

Vaisberg, O. L., G. N. Zastenker, V. N. Smirnov, Z. Nemechek, and I. Shafrankova: 1986b, 'Dynamics of the ion distribution function near the Earth's bow shock (May 11, 1985)'. *Cosmological Research* **24**, 166–176.

Walker, S., H. Alleyne, M. Balikhin, M. Andre, and T. Horbury: 2004, 'Electric field scales at quasi-perpendicular shocks'. *Annales Geophys.* **22**, 2291–2300.

Walker, S. N., M. A. Balikhin, H. S. K. Alleyne, W. Baumjohann, and M. Dunlop: 1999, 'Observations of a very thin shock'. *Adv. Space. Res.* **24**, 47–50.

Wygant, J. R., M. Bensadoun, and F. S. Mozer: 1987, 'Electric field measurements at subcritical, oblique bow shock crossings'. *J. Geophys. Res.* **92**, 11109.